Integrated approach for the development across Europe of user oriented climate indicators for GFCS high-priority sectors: Agriculture, disaster risk reduction, energy, health, water and tourism

Work Package 5

Deliverable 5.2

Report on temporal evolution of the INDECIS-ISD, including the time-emergence of climate-change signals

Albert Ossó[1,2], Richard Allan[1] and Len Shaffrey[1,2], Ana Casanueva[3], Joaquín Bedia[3], Sixto Herrera[3], Mª Dolores Frías[3], Jesús Fernández[3], Antonio S. Cofiño[3], José Manuel Gutiérrez[3], Manuel del Jesús[3], Antonio Espejo[3], Cristina Izaguirre[3], Patricia Bueno[3], Hans Van de Vyver[4], Bert Van Schaeybroeck[4],Pedro M. Sousa[5] and Ricardo M. Trigo[5] , Roberto Coscarelli[6],Tomaso Caloiero[6], Giulio Nils[6]

[1] Department of Meteorology, University of Reading, Reading – United Kingdom

[2] National Centre for Atmospheric Science, University of Reading, Reading – United Kingdom

[3] Universidad de Cantabria, Santander – Spain

[4] Royal Meteorological Institute of Belgium, Brussels – Belgium

[5] University of Lisbon

[6] National Research Council of Italy (C.N.R.)

This report arises from the Project INDECIS which is part of ERA4CS, an ERA-NET initiated by JPI Climate, and funded by FORMAS (SE), DLR (DE), BMWFW (AT), IFD (DK), MINECO (ES), ANR (FR), with co-funding by the European Union's Horizon 2020 research and innovation programme

TABLE OF CONTENTS

1. Introduction

Climate impact indices, such as INDECIS-ISD, are practical tools to assess local and regional sector-specific climate impacts such as floods, droughts, heatwaves or wildfires, among others. Their temporal and spatial variability is, therefore impact-relevant and can be related to climate forcings such as GHG emissions and internal variability. The goal of deliverable 5.2 is to analyse their climatology, temporal evolution, and assess their Time of Emergence (ToE). We have also included an analysis of the scaling properties of extreme precipitation (see appendix 2). Finally an analysis of satellite precipitation trends over Italy is shown in the appendix 3. Much work has also been done analysing the relationship between the indices and patterns of atmospheric circulation, this work will be reported in the deliverable 5.3.

2. INDECIS -ISD

The analysis is performed with a subset of the INDECIS-ISD (table1) developed in WP4 (http://indecis.eu/docs/Deliverables/Deliverable_4.1.pdf). The indices are based on the E-OBS daily observational dataset (v17) on a 0.5x0.5° regular grid for the period 1950-2017.

Index Code	Index Name	Description	Units	Seasonal aggregation function	Climate variables
TP	Total precipitation	Total amounts of precipitation	mm/month	mean	Pr
PVWD	Precipitation fraction due to very wet days	Precipitation at days exceeding the 95percentile divided by total precipitation	%	Mean	Pr
LWP	Longest wet period	Maximum length of consecutive wet days (RR>=1)	days/month	mean	Pr

LDP	Longest dry period	Maximum length of consecutive dry days (RR<1)	days/month	mean	Pr
RR1	Wet day frequency	Nº of days with Pr ≥ 1 mm	Days/season	sum	Pr
SDII	Simple precipitation intensity index	Mean wet-day precipitation	mm/day	mean	Pr
TR	Tropical nights	Nº of days with Tmin>20°C	Days/season	sum	Tmin
SU	Summer days	Nº of days with Tmax>25°C	Days/season	sum	Tmax
FD	Frost days	Nº days with Tmin< 0°C	Days/season	sum	Tmin
ID	Ice days	Nº of days with Tmax<0°C	Days/season	Sum	Tmax

Table 1. Description of considered INDECIS-ISD. Glossary: Pr: Precipitation, Tmax: Maximum temperature, Tmin: Minimum temperature.

3. RESULTS

3.1 Analysis of INDECIS-ISD climatology, variability and trends

Maps of seasonal climatologies (DJF, MAM, JJA, and SON) are calculated by temporally averaging the indices time series at each grid point over the period 1950-2017. Variability is quantified at each grid point as the standard deviation of the corresponding time series. When it helps the interpretation, the standard deviation is normalized by the indices climatological value and the value is expressed as a percentage (check figure captions for details). Years with missing values are ignored in the calculation except if they account for more than 50% of the time steps, in which case the grid point value is left blank.

For the indices TP, PVWD, LWP and LDP we perform a least-squares linear regression at each grid point to assess the tendency maps of the indices. The calculated trends are susceptible to the presence of missing values in the extremes of the series. Therefore, we only show the tendency values at the gridpoints containing complete observations. The significance of the trends is assessed using the methodology outlined by Santer et al. (2000) that accounts for the autocorrelation of the series. For the rest of the indices, the trend analysis is undertaken using the Mann-Kendall's trend test (Kendall Rank Correlation Coefficient, tau), a non-parametric approach that does not make any previous assumption about the distribution of the input data. It is less sensitive to outliers (Hamed and Rao 1998), being therefore better suited for trend detection in the presence of extreme years. In particular, here we use a modified version of the original Mann-Kendall's correlation test (Mann 1945) in which a correction factor is applied to the original variance formulation, accounting for the effective sample size in the presence of temporal autocorrelation, following the definition proposed by Sheng and Wang 2004 (see e.g. Sousa *et al.* 2011 or Bedia *et al.* 2012 for climate applications).

Total precipitation (TP) and precipitation fraction due to very wet days (PVWD)

During autumn and winter, and to a minor degree in spring, the spatial pattern of TP over Europe exhibits a West-East gradient (Fig.1). The largest values of TP are in the west-facing continental coasts, particularly in the Atlantic and the east coast of the Adriatic Sea. This pattern is coherent with the West-East oriented North Atlantic storm track, which favours precipitation over the western coasts when the storms first reach land, especially in places of high orography. Distinctively, during summer, the TP spatial pattern is dominated by a meridional dipole, with dry conditions in South Europe and wet over North Europe possibly reflecting the summer poleward migration of the storm track. Large values of TP are also found over the Alpine regions all year round, with the most significant values found during summer possibly due to the intense convection events in mountain regions during this season. The interannual variability of TP (expressed as a percentage of the climatological value) is notably homogeneous over Central and North Europe with sizes of about 30% the climatological values. During summer and winter, TP variability is higher over Southern Europe (>50% the climatological values) coinciding with the lowest values of TP (Fig.1).

In wintertime, the spatial pattern of TP trends exhibits widespread drying south of the 47° latitude band (except for the oriental Alps and some parts of the Balkans) and a wetting trend north of this latitude (Fig.1, right column). Note however that in Southern Europe the trends are generally not significant due to the large interannual variability over this area (see Fig.1 right column). In spring, the meridional winter dipole is no longer apparent, and the tendencies are positive overall Europe although only statistically significant over Scandinavia, Scotland and the Oriental Alpine region. Fig.2 shows winter spatially average TP timeseries over the indicated regions with its linear trends. In winter, TP has increased by about 2.6% per decade over Scandinavia, about 4.2%/decade over the UK (Fig.2a) and has decreased by about -2%/decades in the Iberian Peninsula although the trend is not statistically significant. The larger areas of North Europe and South Europe also exhibit a wetting and drying trend respectively although their magnitudes are smaller. Summer trends have the same sign of those of winter but their magnitude is smaller (Fig.3) and only statistically significant over Scandinavia and UK. Time series for all the seasons are shown in the appendix 1.

The largest values of PVWD are found over central Europe all year round and the lowest over the Iberian Peninsula and the Balkans (Fig. 4). The most substantial spatial differences are during the summer season when PVWD accounts only for about 4% of TP in Iberia but about 18% in Central Europe. The interannual variability of PVWD is notably homogeneous both seasonally and spatially with values of about ~10% the PVWD climatological value through the year. PVWD tendencies have been expressed in PVWD units (%) per decade, without normalization. There has been a widespread increase of PVWD over Europe in all seasons (i.e. the fraction of the total precipitation due to very wet days has increased) although some regional differences are apparent (Fig.4). The largest trends are observed over Scandinavia and Scotland throughout the year and over the Alps in summer while a year-round reduction is apparent in North Italy. Figure 5 shows spatial average PVWD timeseries for winter and summer. In winter all the regions analysed except the Iberian Peninsula show a positive and statistically significant trend in PVWD, being the largest in Scandinavia. In summer, the trends are weaker and only significant over Scandinavia (1.18%/decade).

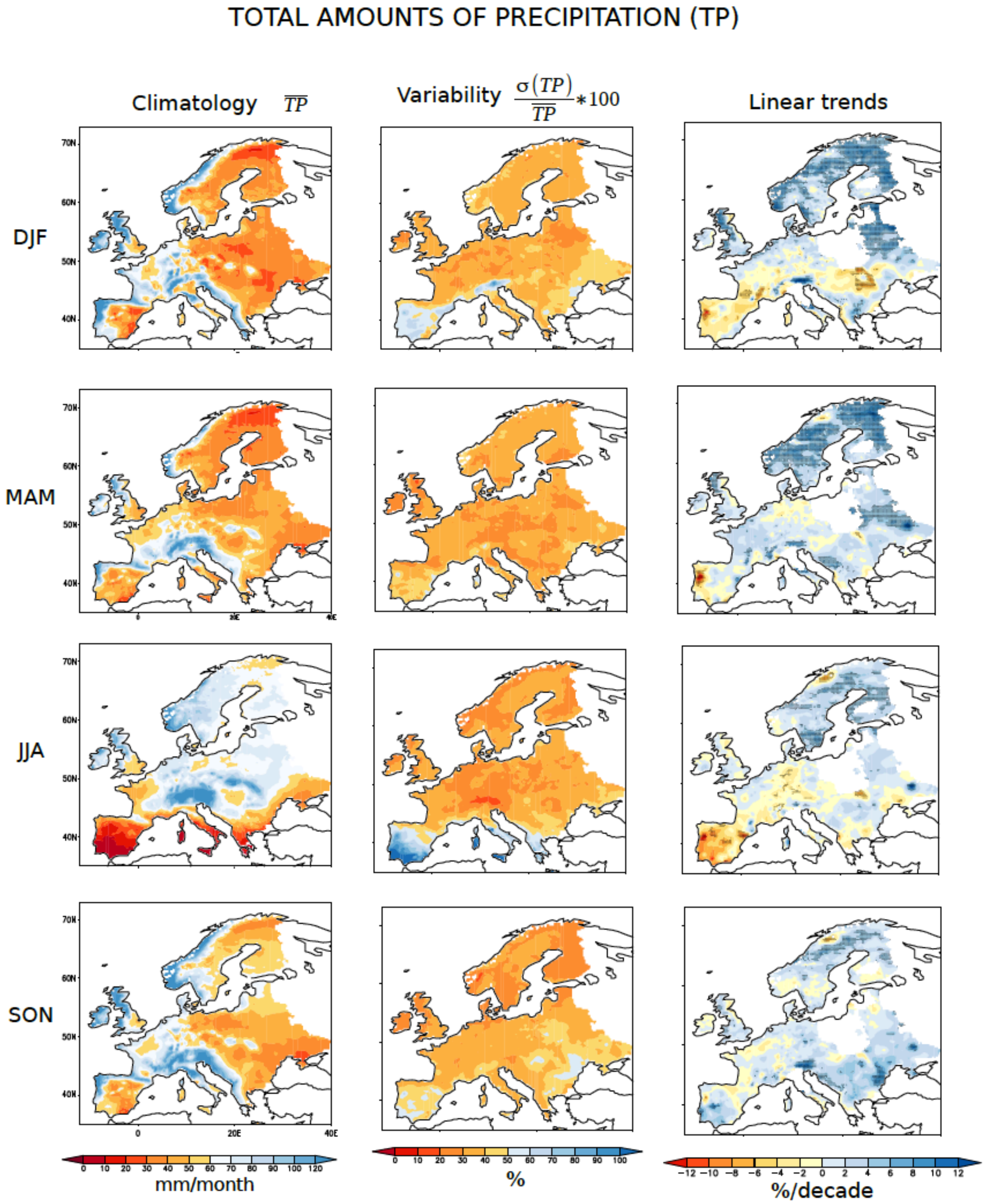

Figure 1: Left column: Seasonal climatology. Central column: Seasonal interannual variability expressed as a percentage with respect to the climatology. Right column: Observed tendency for the 1950-2017 period. The regression coefficients have been normalized by the TP climatological value and expressed

as a percentage. Grid points with incomplete observations are left white shaded. Stippling indicate regression coefficients statistically significant at the 95% level.

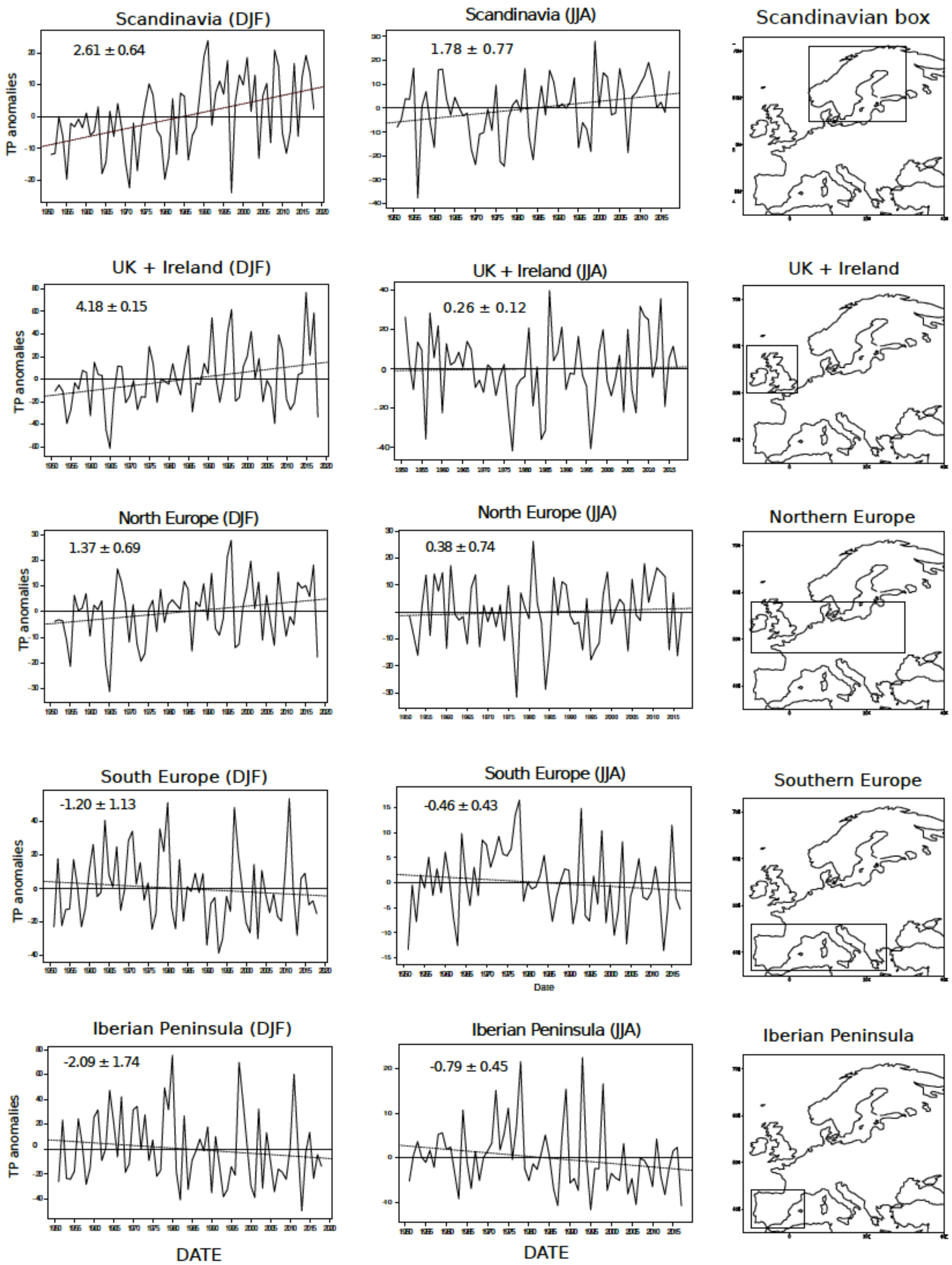

Figure 2: Observed winter and summer TP anomalies (mm/month) spatially averaged over the indicated geographical regions (right column) and estimated linear trends for the period (1950-2017) expressed as a percentage of the climatology (%/decade). The standard error of the regression coefficient is also shown.

Precipitation due to very wet days (PVWD)

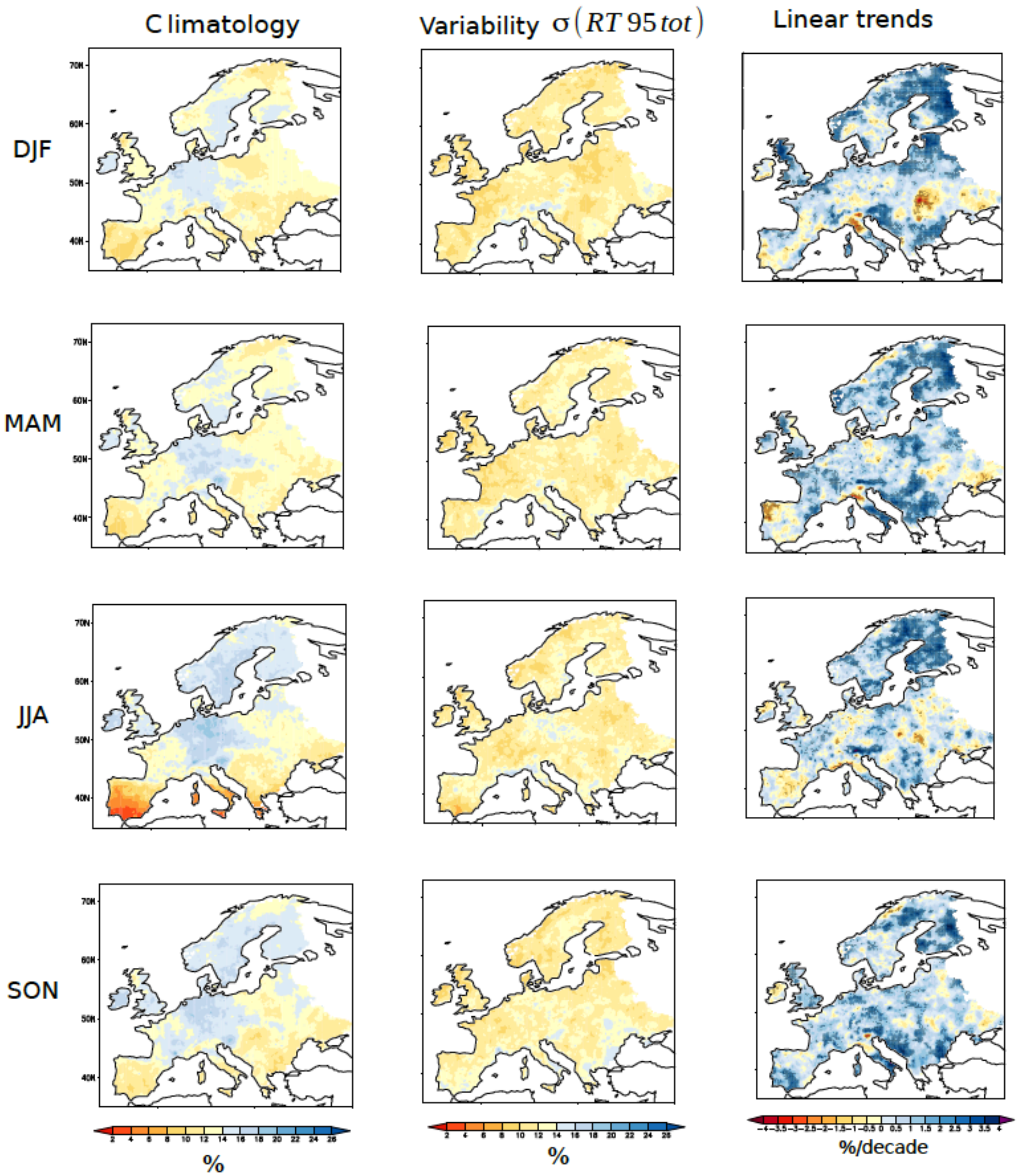

Figure 3: Left column: Seasonal climatology. Central column: Seasonal interannual variability expressed in PVWD units (%). Right column: Observed tendency for the 1950-2017 period. The regression coefficients are expressed in PVWD units (%) per decade (%/decade). Grid points with incomplete

observations are left white shaded. Stippling indicate regression coefficients statistically significant at the 95% level.

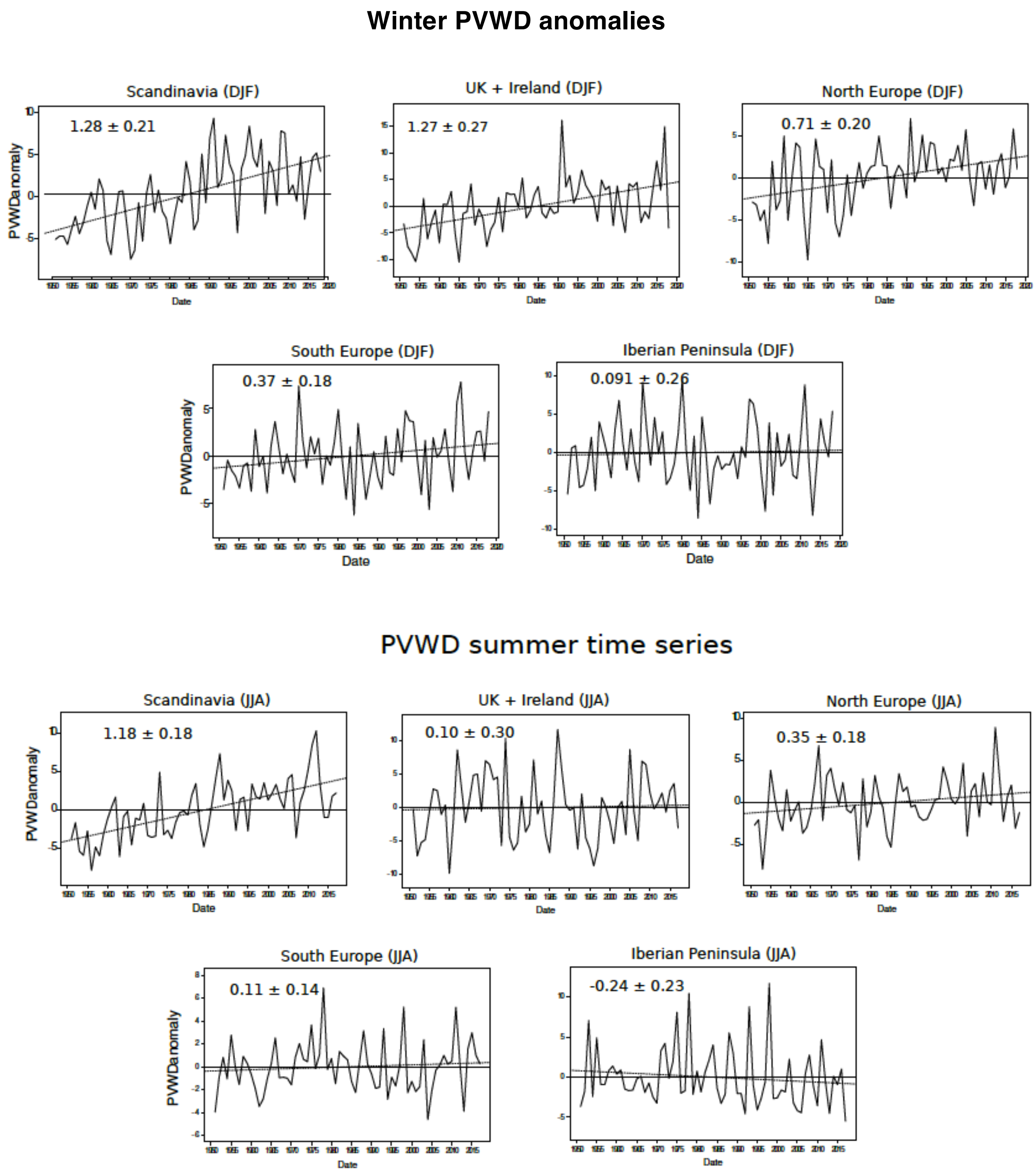

Figure 4: Observed winter and summer PVWD anomalies (%) spatially averaged over the indicated geographical regions (see Fig.A1) and estimated linear trends for the period (1950-2017). The regression coefficients are expressed in PVWD units (%) per decade (%/decade). The standard error of the regression coefficient is also shown.

The longest wet period (LWP) and the longest dry period (LDP)

Similarly to TP, during winter, autumn and spring the spatial pattern of LWP is characterized by a west-east gradient, while in summer, a meridional dipole prevails with larger values over North Europe and smaller over South Europe (Fig.5). Over the western coasts, LWP values are about 8-10 days long while during summer over South Iberia LWP is not longer than one day. The interannual variability of LWP is notably homogeneous over Central and North Europe with values of about 25% the size of LWP climatology. During summer and winter, the highest values are over Southern Europe (>50% of the LWP climatology) coinciding with the lowest climatological values of LWP and TP. The seasonality and the spatial patterns of LDP look like the opposite version of LWP (Fig.6). The largest spatial differences are observed in summer with dry periods longer than 30 days in South Iberia and shorter than six days in the Alps and the West coast of Scandinavia.

We express LWP and LDP tendencies on their original units (days), without normalization. In this way, the temporal changes can be more directly related to impacts. In winter, LWP has increased over Western Scandinavia, North-East Europe, and the UK, and has decreased over the Iberian Peninsula and Central Europe (Fig.5). Although some values are statistically significant, these are generally small and do not reach the unit in any case. In spring, the spatial pattern resembles that of winter but with smaller magnitudes. In summer and autumn, the tendencies are small and generally no statistically significant. In winter, LDP tendencies depict a clear North-South dipole pattern, with negative trends in Scandinavia and North-East Europe and positive over Southern Europe (Fig.6). Interestingly, during summer there is an overall positive trend over Europe except in Scandinavia. Since there is no trend in summer LWP, these positive trends cannot be explained as changes in the velocity of storm propagation (which could have been the case if LDP tendencies would look like the opposite version of LWP) suggesting that a feedback might be increasing the length of the dry episodes once these are dynamically established (e.g., via land-atmosphere processes).

Figure 7 shows spatially averaged timeseries for LWP and their trends. Note that we only show the timeseries that exhibit statistically significant trends. The rest of time series are shown in appendix 1. In winter, significant tendencies are observed over Scandinavia (0.11 days/decade) and the Iberian Peninsula (-0.17 days/decade). In summer, the only statistically significant tendency is observed over the UK and Ireland with a reduction of LWP of -0.17 days/decade.

The longest wet period (LWP)

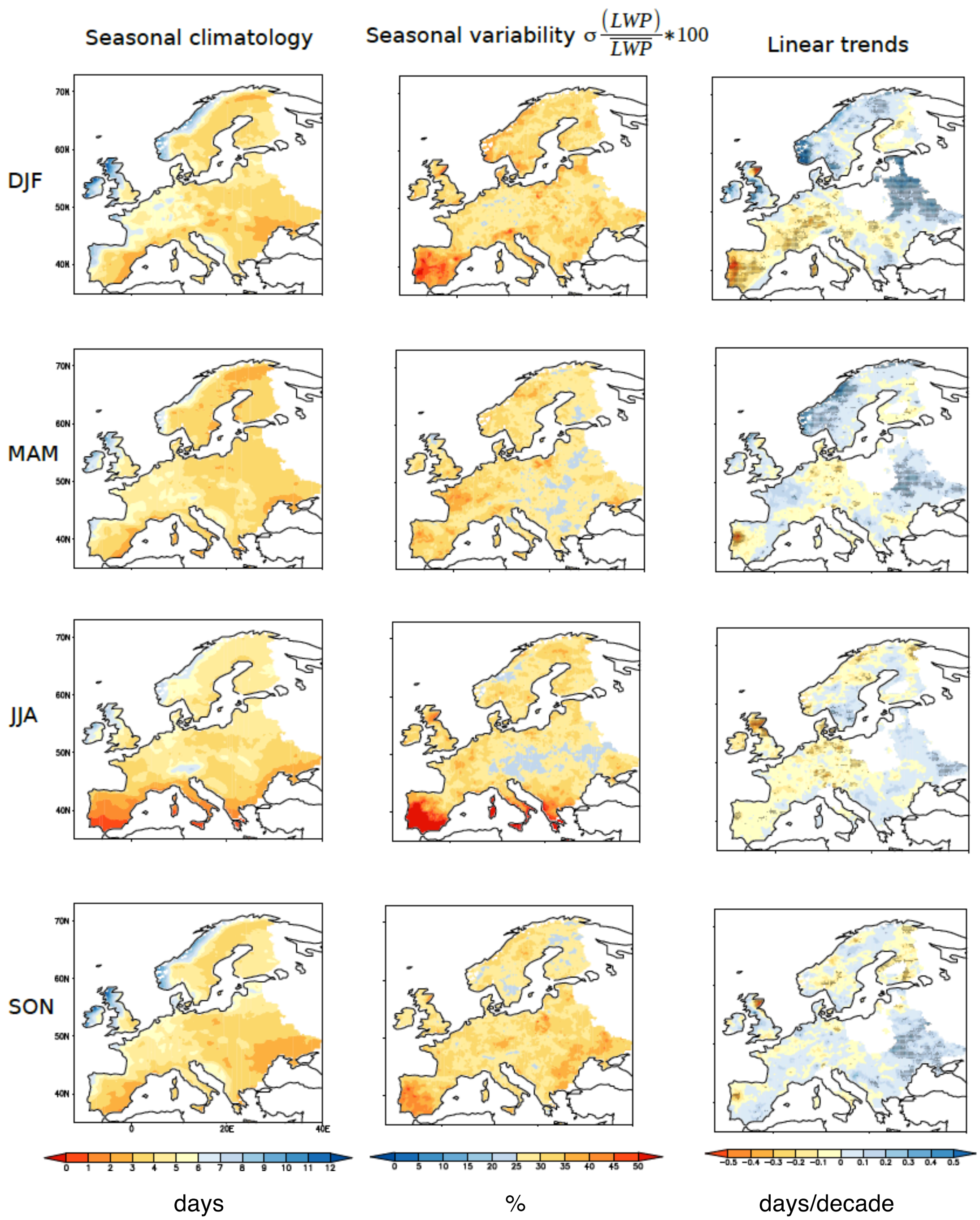

Figure 5: Left column: Seasonal climatology. Central column: Seasonal interannual variability normalized by LWP climatology and expressed as a percentage (%). Right column: Observed tendency for the 1950-2017 period. The regression coefficients are expressed in LWP units (days) per decade. Grid points with incomplete observations are left white shaded. Stippling indicate regression coefficients statistically significant at the 95% level.

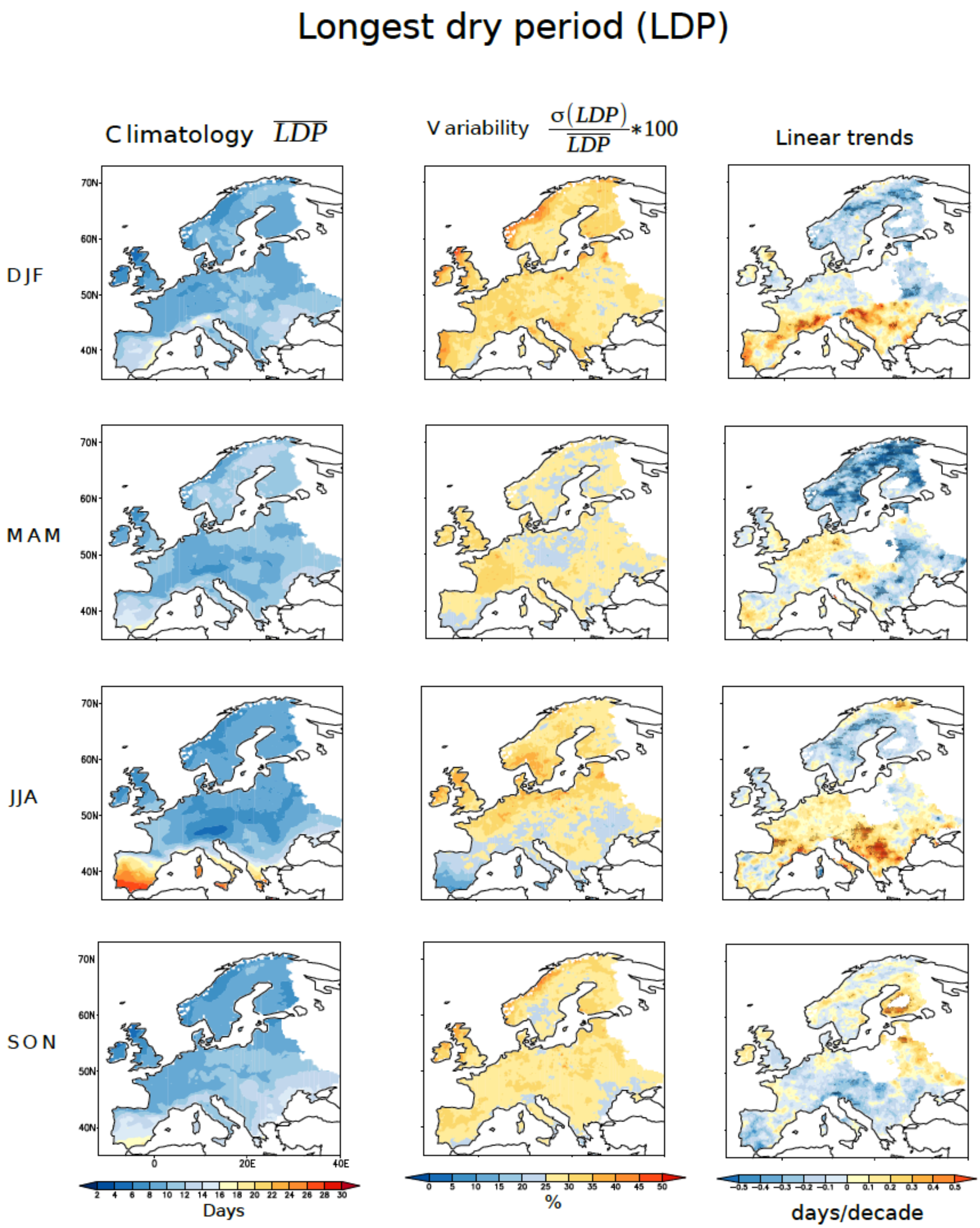

Figure 6: Left column: Seasonal climatology. Central column: Seasonal interannual variability normalized by LDP climatology (%). Right column: Observed tendency for the 1950-2017 period. The regression coefficients are expressed in LDP units (days) per decade. Grid points with incomplete observations are left white shaded. Stippling indicate regression coefficients statistically significant at the 95% level.

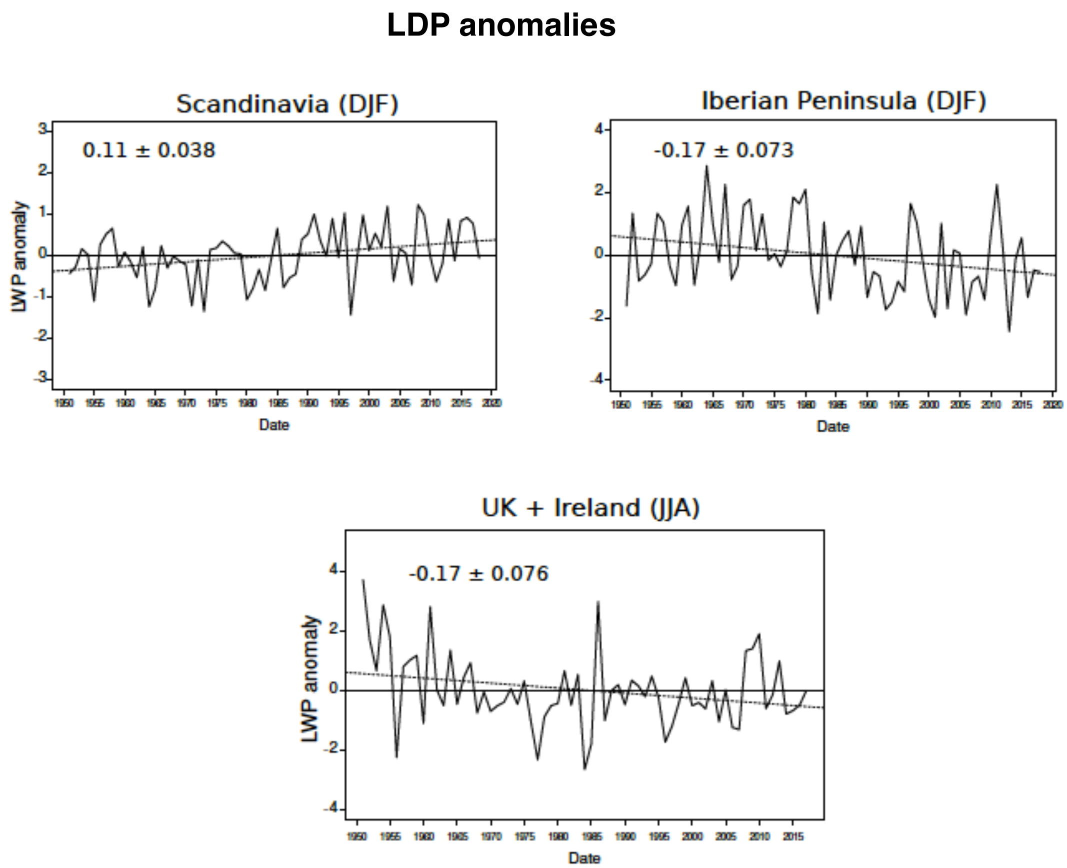

Figure 7: Observed winter and summer LWP anomalies (days) spatially averaged over the indicated geographical regions (see Fig.A1) and estimated linear trends (days/decade) for the period (1950-2017). The standard error of the regression coefficient is also given.

Frequency of wet days (RR1) and Wet-day intensity (SDII)

The European areas with larger frequency of wet days (RR1, Fig. 8) are found in the Atlantic watershed, in particular, along the Scandinavian coast and the British Isles, throughout the year. Central Europe and northwestern Russia present RR1 of more than 35 summer days on average, and up to 60 days in the Alpine ridge. Larger variability is accordingly found in the areas with larger RR1. Wet-day intensity (Fig.9) presents the largest values in the Norwegian coast and northwest of Spain in winter, whereas higher intensities are found in the Alpine ridge and the Mediterranean area in the other three seasons. SDII in the Gulf of Genoa and Gulf of

Venice amounts to more than 9mm on average along the four seasons. Autumn precipitation is also characterized by high SDII in south-western Iberian Peninsula and along the Mediterranean region.

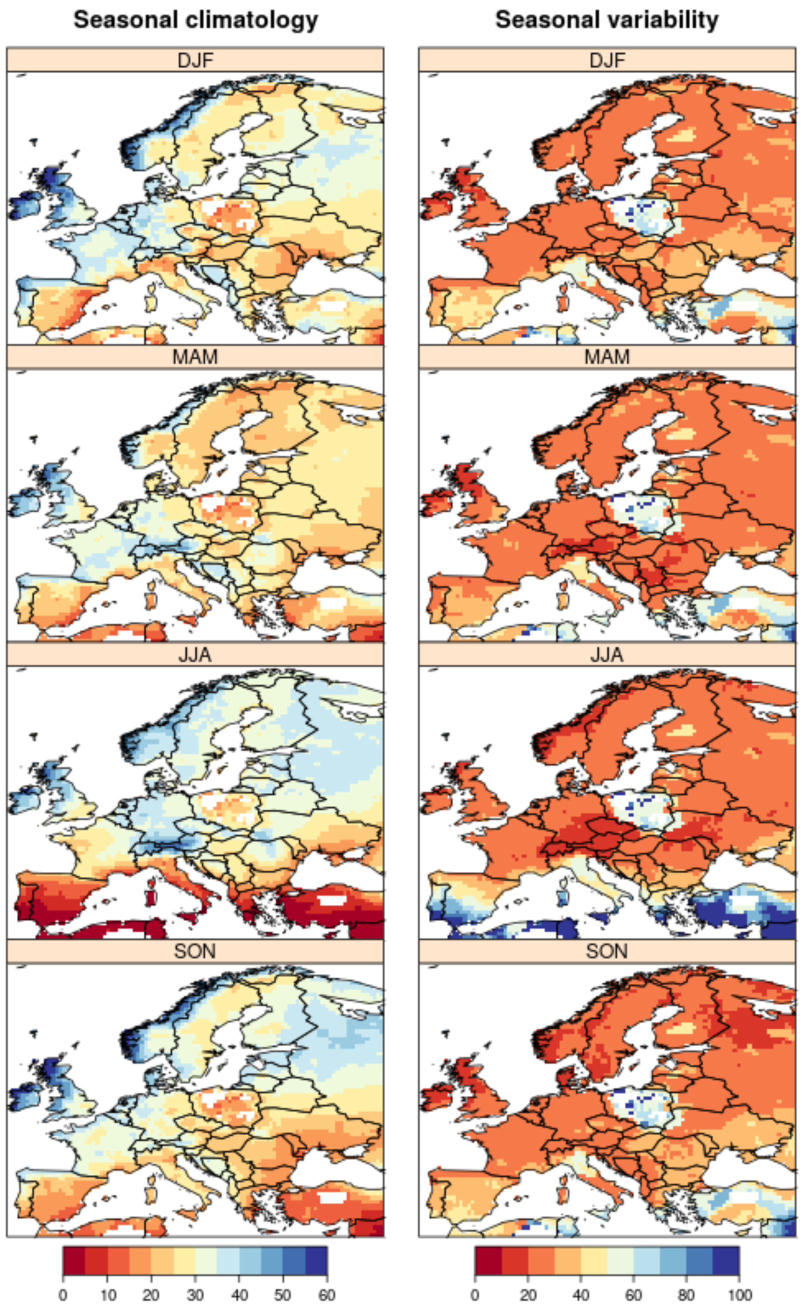

Figure.8: Seasonal climatology (days/season) and variability (%, see text) of RR1.

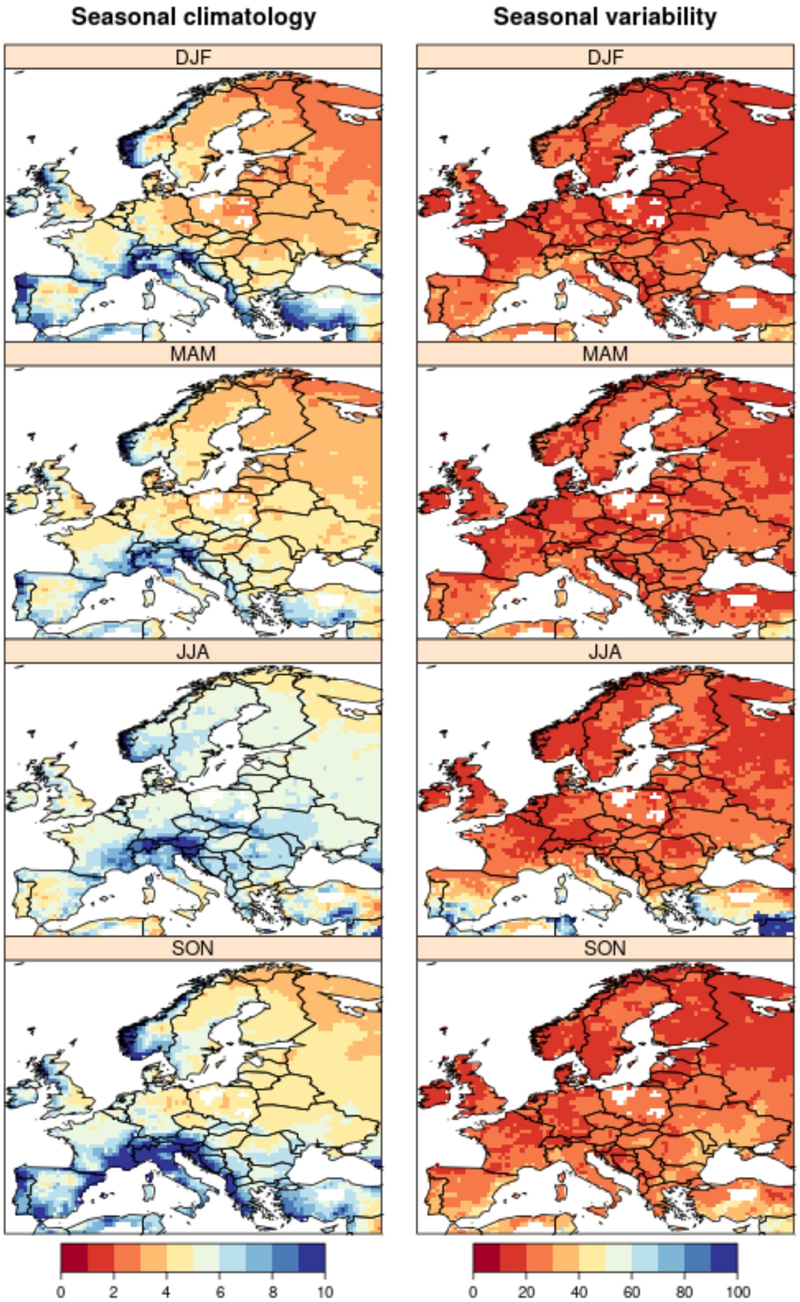

Figure.9 Seasonal climatology (mm/day) and variability (%) for SDII.

RR1 has specially increased in northeastern Europe in winter and decreased in scattered regions in Central Europe and Italy throughout the year (Fig.10). SDII presents an overall increase in the four seasons, except for a decrease in northwestern Iberia in spring (Fig.11). Interestingly, positive trends are found in areas with the largest accumulations in the intermediate seasons, such as the Alpine ridge and the Adriatic coast in spring and autumn and southwestern Iberia in autumn (in agreement with Casanueva *et al.* 2014).

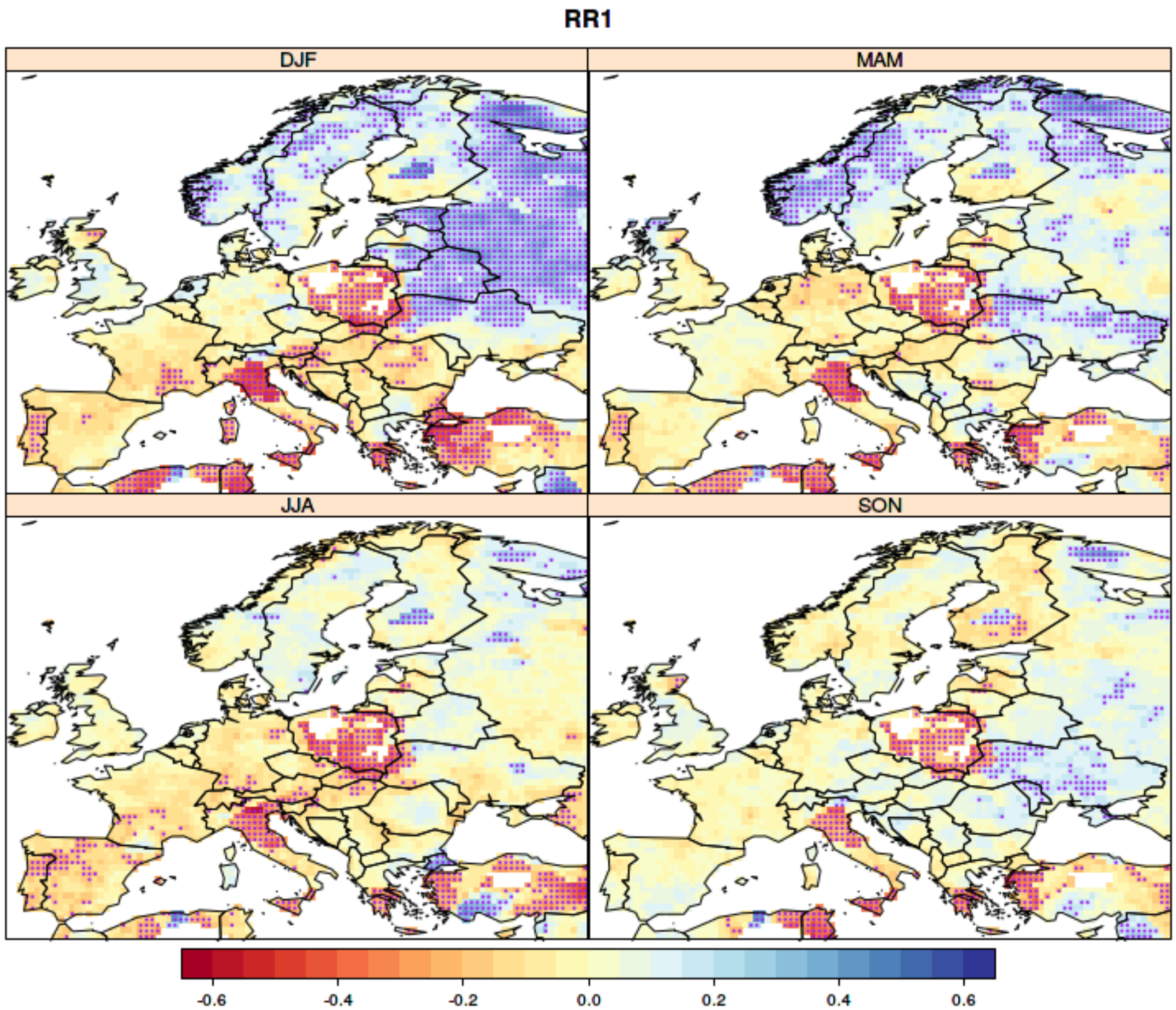

Figure.10 Kendall's Tau coefficients for RR1 in the period 1950-2017. Statistically significant values (p-value < 0.05) are depicted in purple.

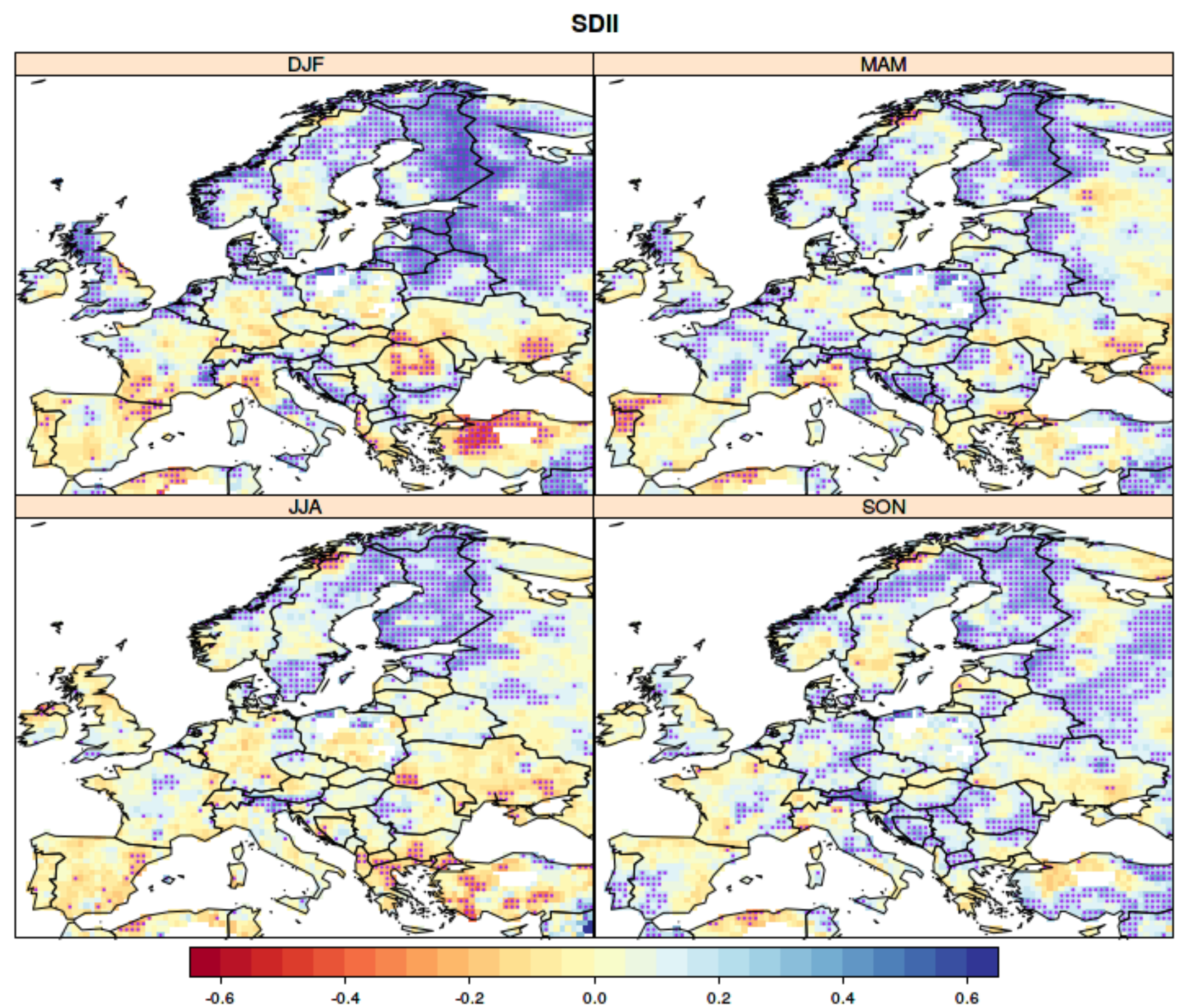

Figure.11 As Fig.10 but for trends in SDII.

Tropical nights (TR) and summer days (SU)

Tropical nights are, on average, detected during summer time along the Mediterranean and the Black Sea (Fig.12), with values of more than 12 days (on average) in southwestern Spain and a large part of Italy. The variability of this index is very large, being driven by very extreme years (e.g. 2003, 2015). Summer days are not only found in summer. Up to 30 and 50 summer days are also found in spring and autumn in some hot spots in the south of the continent (Fig.13). Interannual variability is small in these areas. In summertime, there are more than 65 SU days on average in southern Europe and up to 40 SU days in the lowlands of Central Europe.

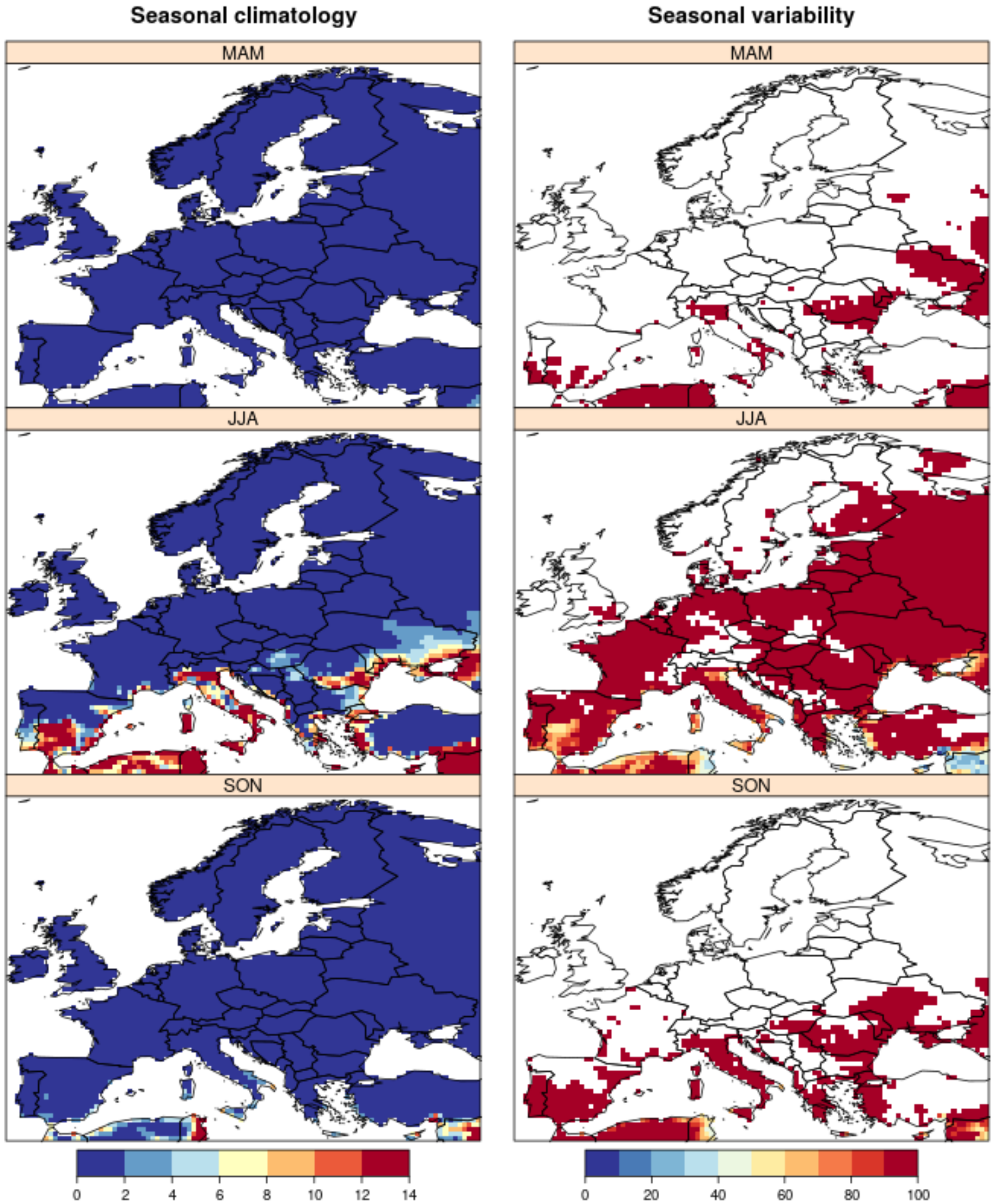

Figure 12: Seasonal climatology (mm/day) and variability (%) for TR.

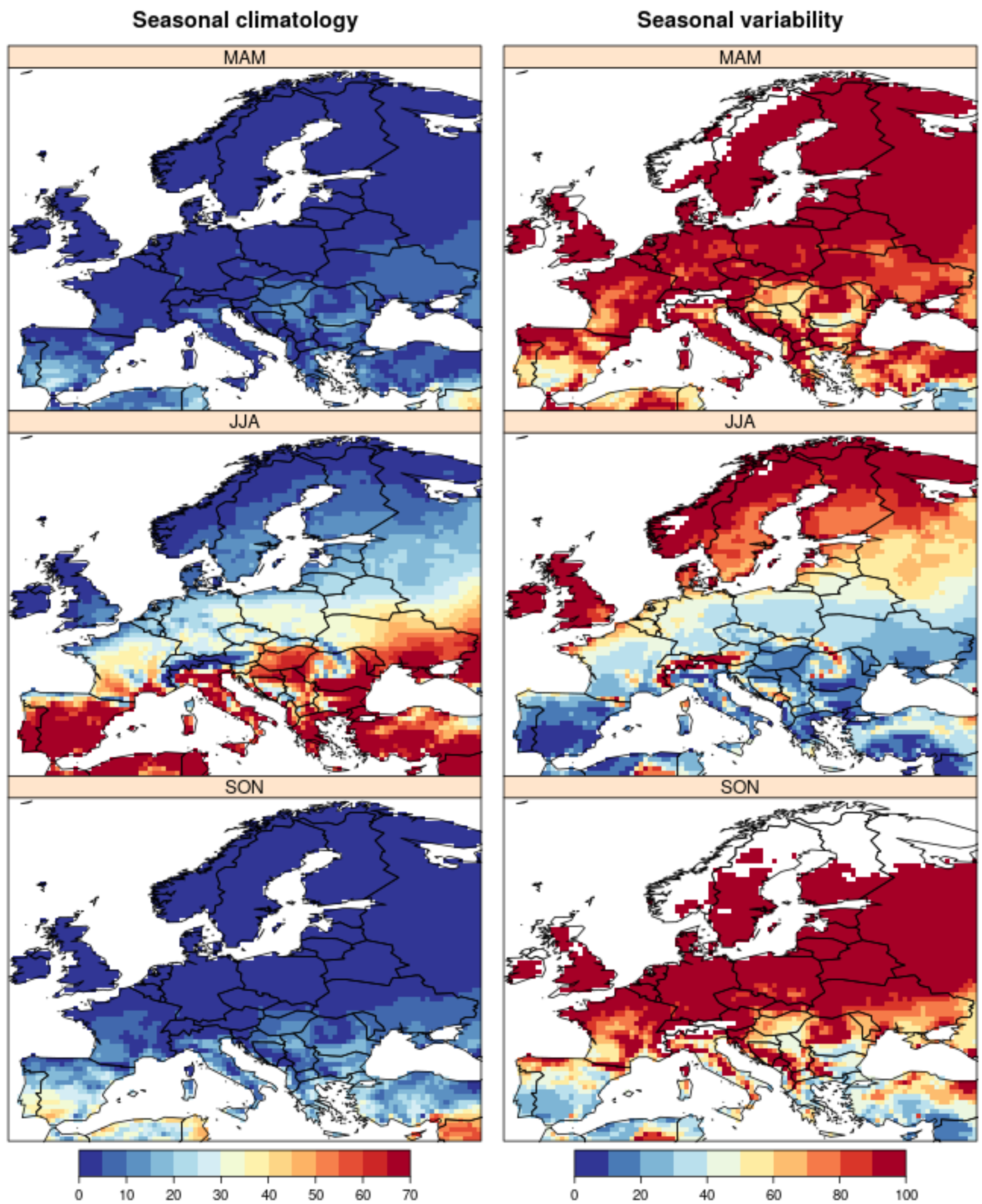

Figure 13: Seasonal climatology (mm/day) and variability (%) for SU.

TR and SU present an increasing and significant trend especially in the areas with the largest climatological values (Fig.14, 15). An increase of SU in the intermediate seasons is also noticeable in Iberia and France.

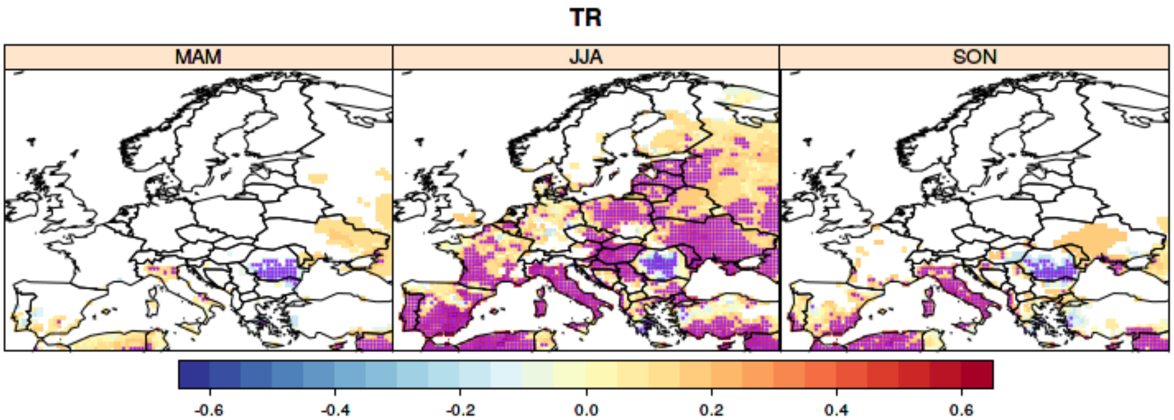

Figure 14 Kendall's Tau coefficients for TR in the period 1950-2017. Statistically significant values (p-value < 0.05) are depicted in purple.

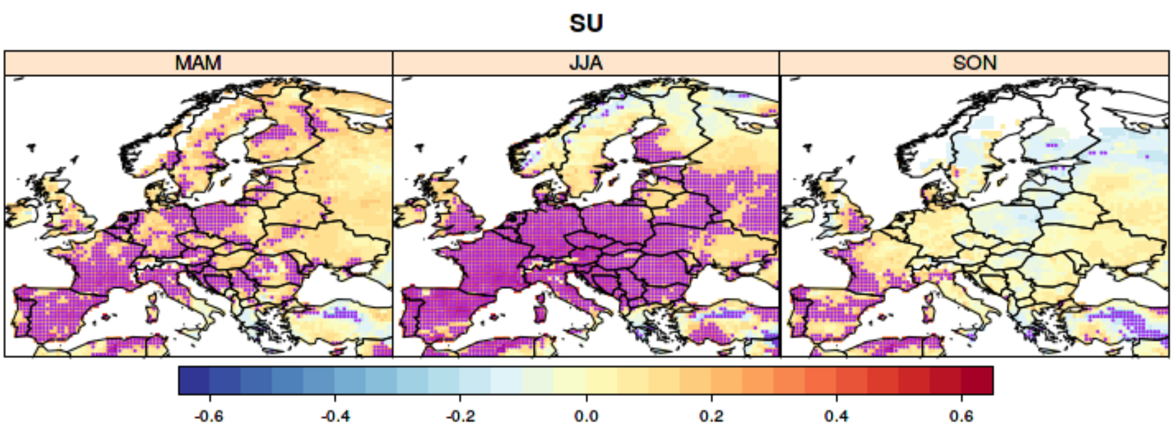

Figure 15 As Fig.14 but for SU trends.

Frost days and ice days

Similar spatial pattern is found for frost days and ice days (Figs. 16,17), depicting an orographic pattern. The largest values occur in winter (more than 50 FD and 30 ID in large parts of the continent, increasing eastwards), although some FD and ID are also found in spring and autumn (around 50 FD and 30 IC in Scandinavia in autumn).

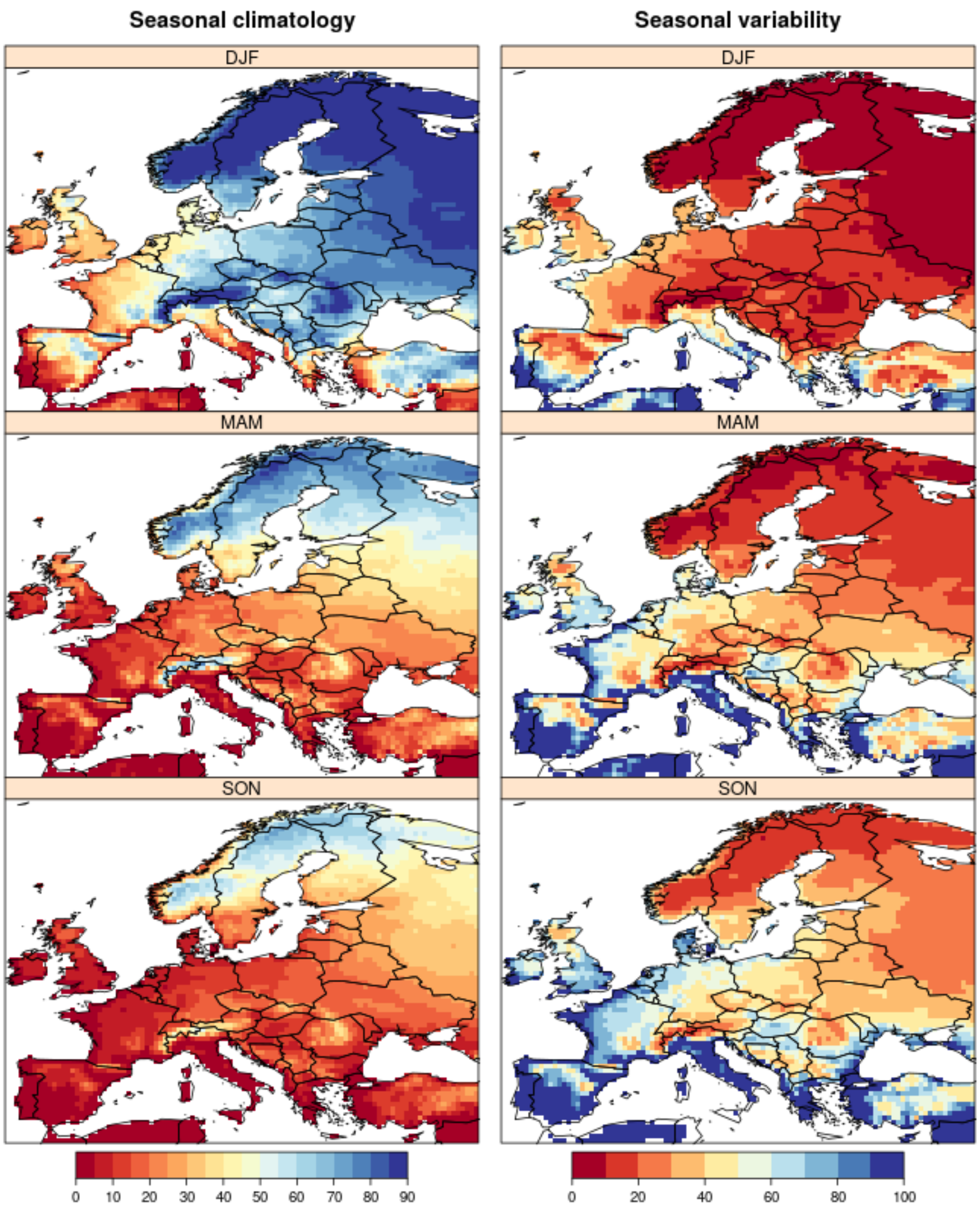

Figure 16: Seasonal climatology (days) and variability (%) for FD.

.

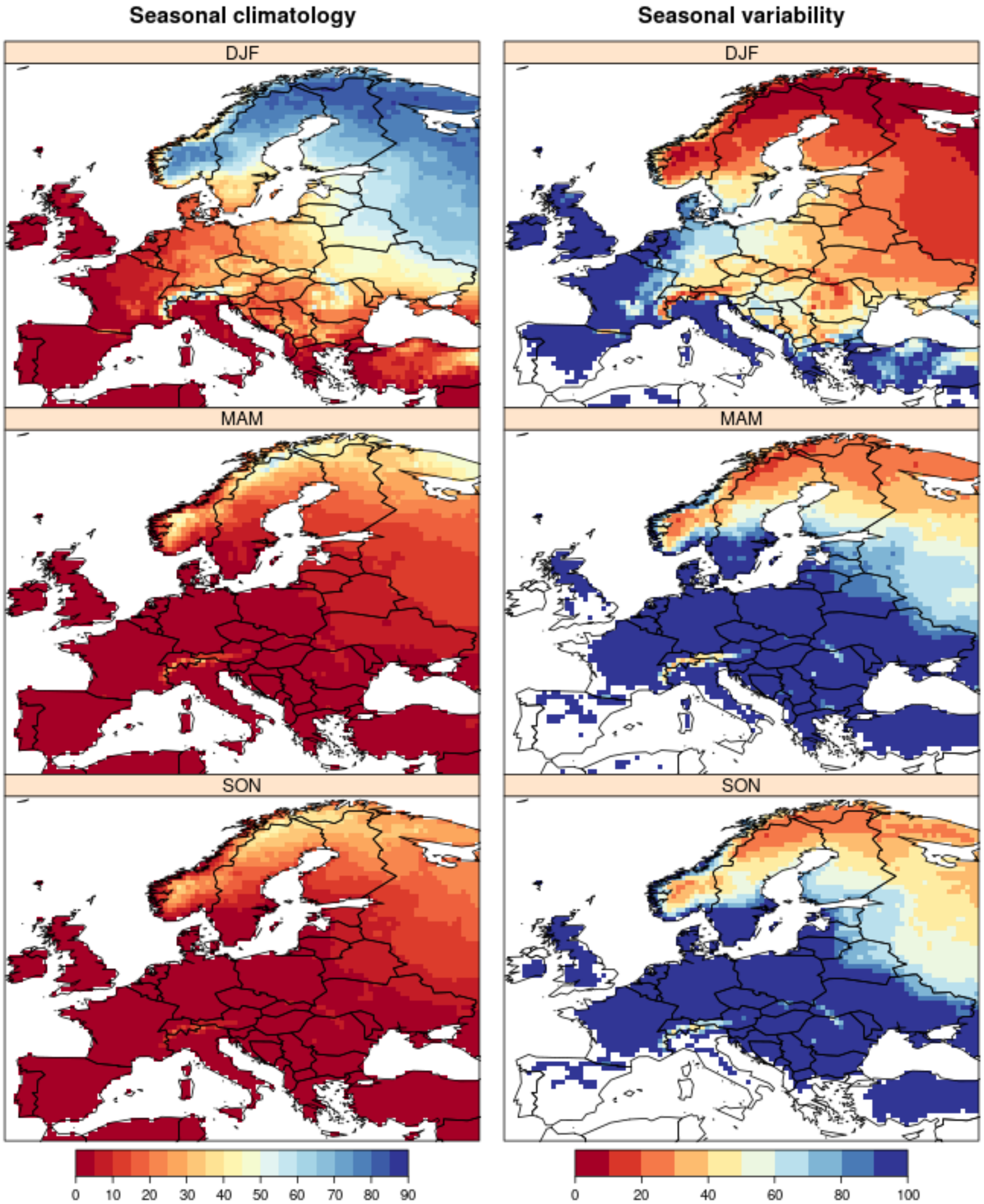

Figure 17: Seasonal climatology (days) and variability (%) for ID.

Trends is cold extremes (FD and ID) are not statistically significant in the areas and seasons where the largest values occur (Fig.18, 19).

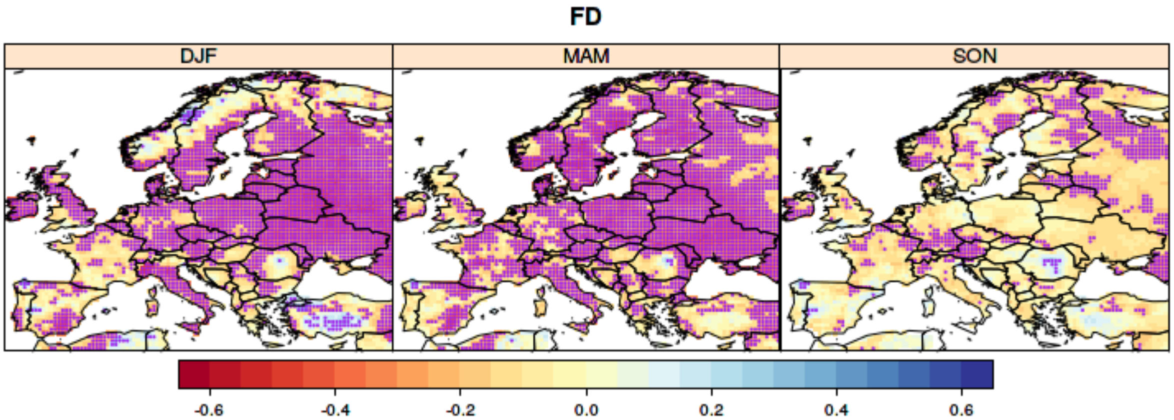

Figure 18: Kendall's Tau coefficients (days/year) for FD in the period 1950-2017. Statistically significant values (p-value < 0.05) are depicted in purple.

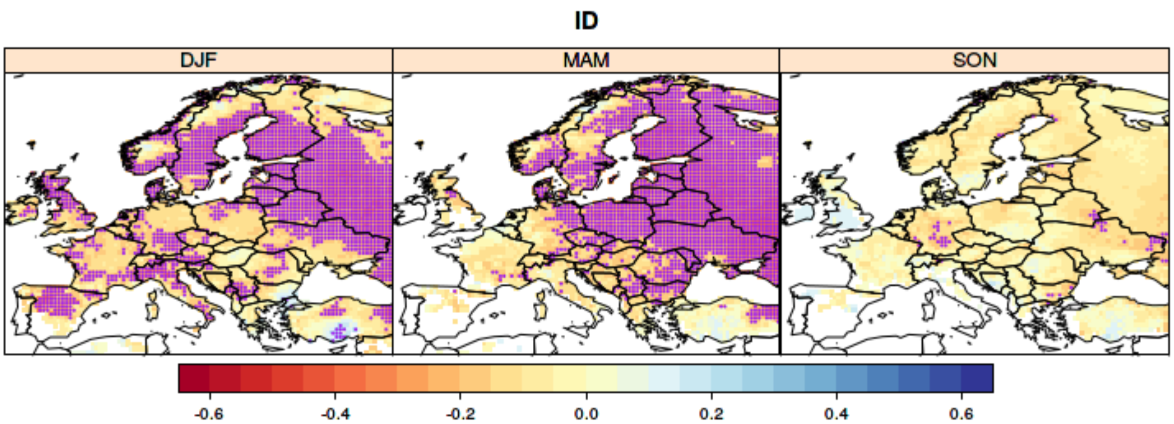

Figure 19: As Fig.18 bur for trends in ID.

3.2 Time of emergence (ToE) of INDECIS-ISD

The ToE is defined as the time or date at which the signal of climate change emerges from the noise of natural variability. The ToE is a critical magnitude for climate change attribution, and it is especially relevant for risk assessment (e.g., Hawkins and Sutton 2012). Most of the existing literature on the impacts of climate change focus on the absolute magnitude of change, however, in many practical situations is the magnitude of change relative to its background variability that is most relevant. The natural systems are inherently adapted to the local background level of variability and its when the signal surpasses this range that the system can get out of balance. Climate change is a global phenomenon, but their impacts differ from region to region and also from one season to another. Mitigation measures should ideally be region and season-specific. Therefore, providing a comprehensive estimation of the local ToE of climate impact indices as a function of the season is highly valuable for the stakeholders.

ToE calculation

Estimating the ToE of a climate signal requires estimating the climate change signal (S) and the natural variability or noise (N). The ToE is then defined as the first year in which the S/N ratio crosses a particular threshold. Different thresholds such as 1or 2 can be used. We choose S/N>1 on this particular work. We compute the signal and noise following the methodology proposed by Ed Hawkins (e.g.,https://www.climate-lab-book.ac.uk/2014/signal-noise-emergence/). It can be described as follows:

1. We fit a quadratic polynomial to the indices anomalies at each grid point over the entire period (smooth fit) (Fig. 20a).

2. The difference in the smoothed fit values between 1950 and 2017 defines the signal.

3. The standard deviation of residuals from a smooth fit defines the noise (Fig. 20b).

4. Signal-to-noise is simply the ratio of signal and noise.

5. The year of emergence is the first year when various S/N thresholds are permanently crossed.

Like for the tendency calculations, we only show values of the ToE analysis at the gridpoints that contain complete observations

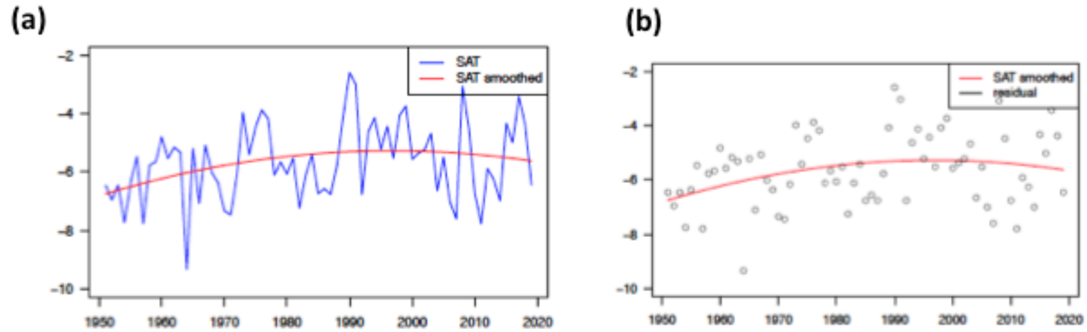

Figure 20: (a) Example of a smooth fit of surface temperature anomalies at a random grid point. (b) The standard deviation of residuals from a smooth fit defines the noise.

The section 3.1 on tendencies provides a picture of the overall indices change. In this section, we extend this analysis by investigating how substantial are these changes with respect to the indices internal variability. A signal larger than the internal variability suggests that the impact of climate change is already noticeable.

Total precipitation (TP) and the fraction of precipitation due to very wet days (PVWD)

In all seasons, the spatial pattern and the size of the noise scale with the signal. That is, generally, the areas with higher noise coincide with the areas with the higher signal in absolute value (negative or positive). Therefore, the TP signal-to-noise (S/N) ratio spatial structure strongly resembles the spatial structure of the signal (Fig.9). In winter and summer, the S/N ratio is positive over North Europe and the Oriental Alps and negative in South Europe. In spring and autumn, positive S/N ratio is more widespread. Although the S/N ratio is larger than 1 (our chosen threshold) in many locations, the signal has only consistently emerged over the Oriental Alps region where the value of the S/N ratio is consistently larger than one all year round after the years 2010-2015. Note that a S/N ratio larger than 1 is a necessary but not sufficient condition for the signal to emerge since the year of emergence is defined as the first year when the S/N thresholds are permanently crossed. Like for TP, the PVWD S/N ratio structure is similar to that of the signal (Fig.10). Overall, the ratios are positive all year round, but the ratios magnitudes are smaller than for TP. The signal has emerged over a small area over the Oriental Alps in summer, spring and autumn and over Greece and some areas of the Balkans during the transitions seasons, spring and autumn. However, caution is needed over the Balkans since spurious temperature trends reported over this area (*Gerard van der Schrier* personal communication) cast doubt on the reliability of precipitation time-series.

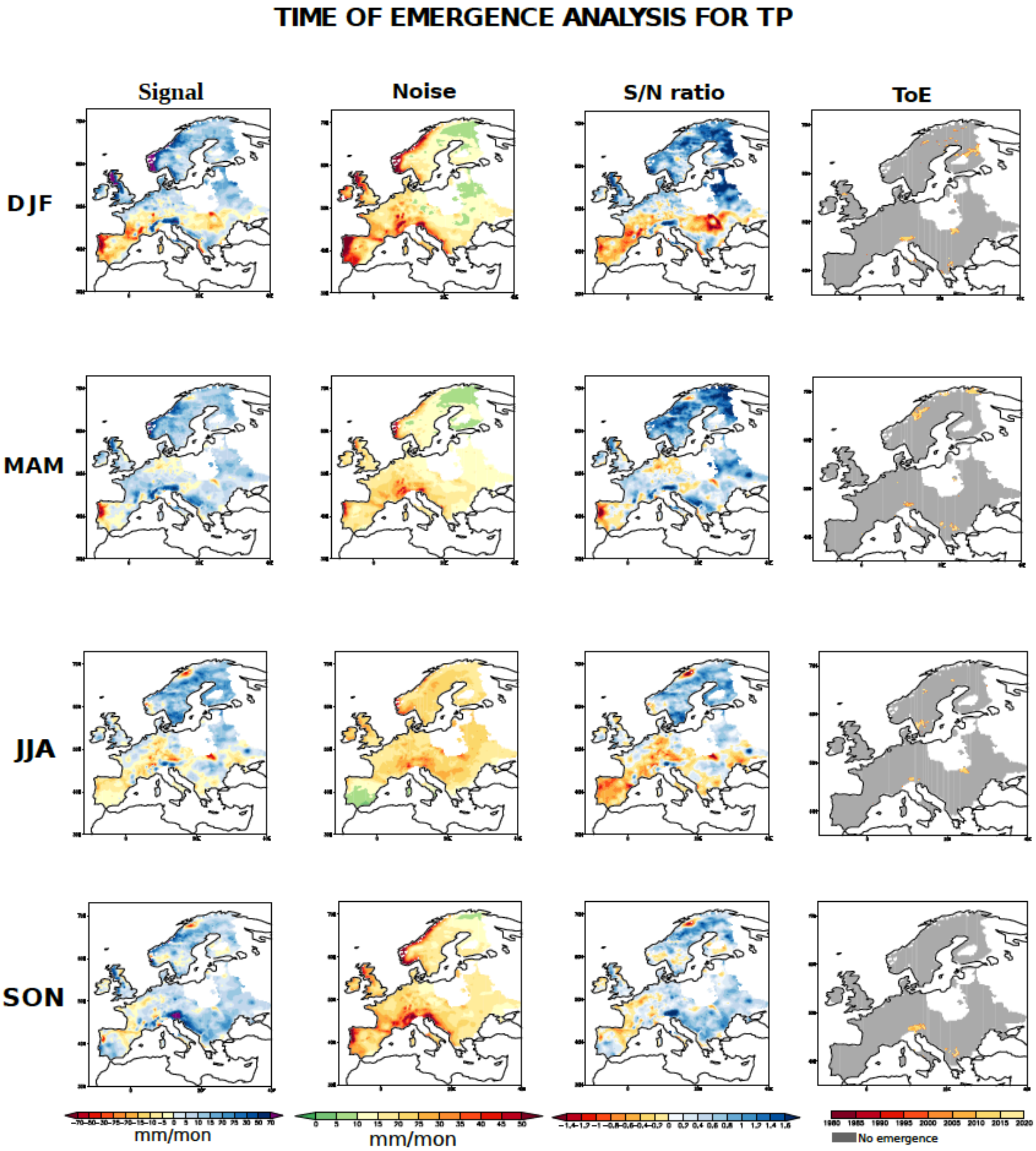

Figure 21: From left to right column: Signal, noise, signal-to-noise ratio and Time of Emergence.

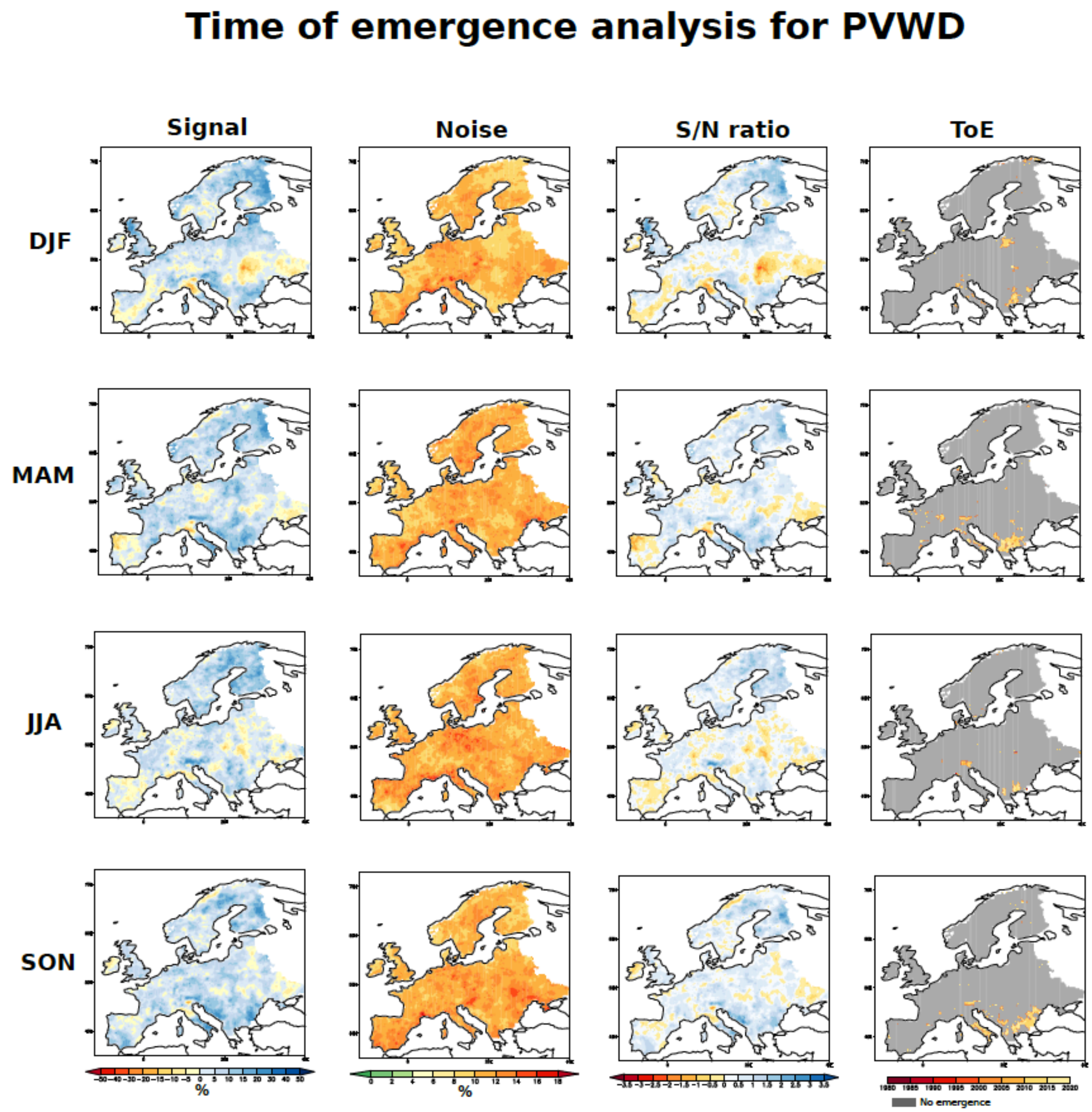

Figure 22: From left to right column: Signal, noise, signal-to-noise ratio and Time of Emergence (see section 2 for details on the calculation).

<u>The longest wet period (LWP) and the longest dry period (LDP)</u>

Overall, the signal in LWP has not emerged from the background variability anywhere in Europe at any season (Fig.23). The strongest signals are in wintertime when LWP decreased over Central and Southern Europe and increased over the UK, NW Europe and Scandinavia. The strongest signal is seen over Portugal where the LWP have reduced for up to 3 days. The areas with the stronger signal are also the areas with the stronger variability. The MAM signal resembles DJF but weaker and in summer and autumn the signal is in general weak and no clear pattern is apparent.

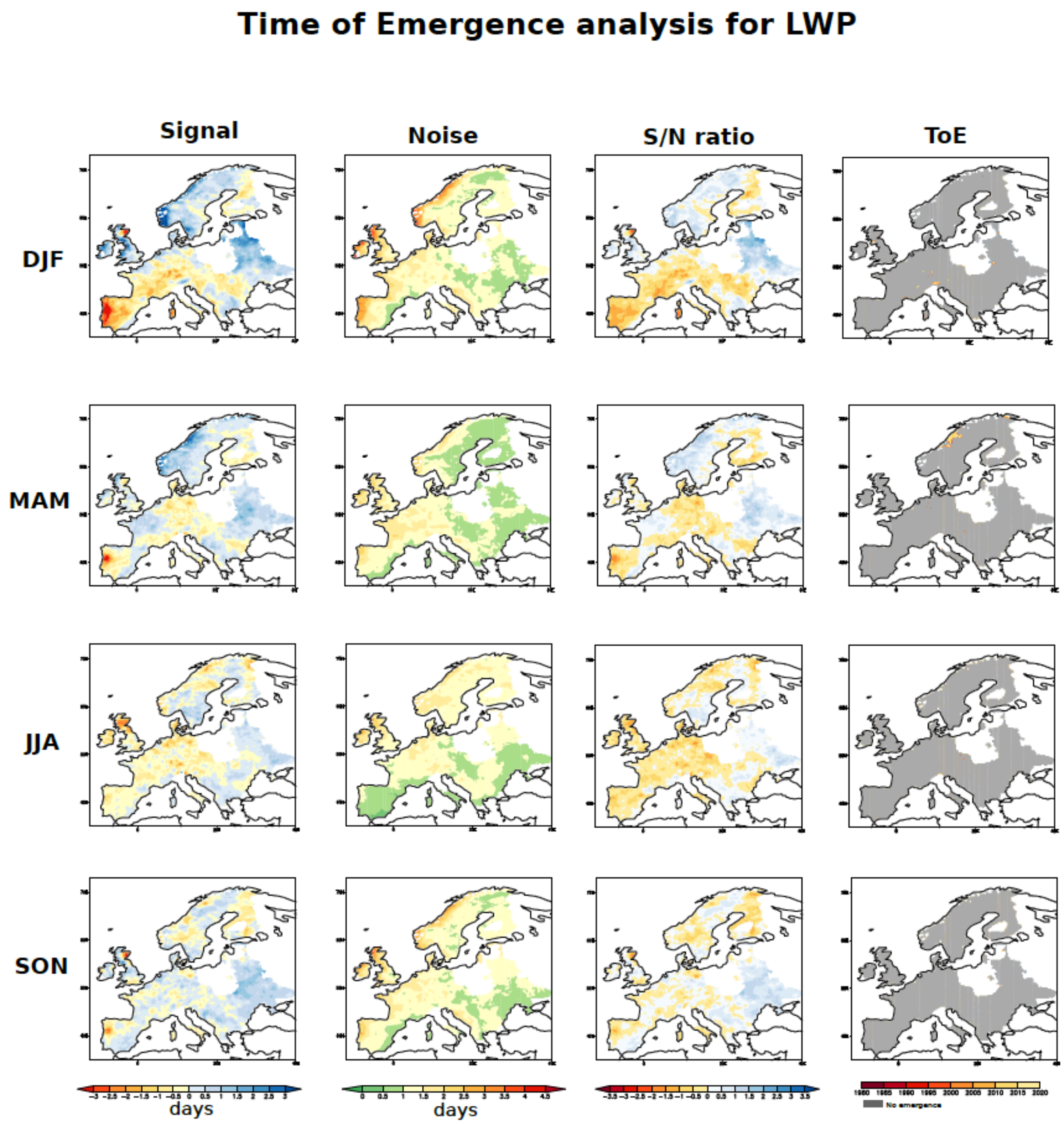

Figure 23: From left to right column: Signal, noise, signal-to-noise ratio and Time of Emergence (see section 3.2 for details on the calculation).

As for LWP, the LDP signal has generally not emerged except for a small area over the Balkans during summer, where the LDP has increase up to 6 days (Fig.24). In wintertime thee general tendency is to an increase of LDP over Southern Europe and to a decrease over North Europe. During spring and summer LDP extends north but the signal is overall weak.

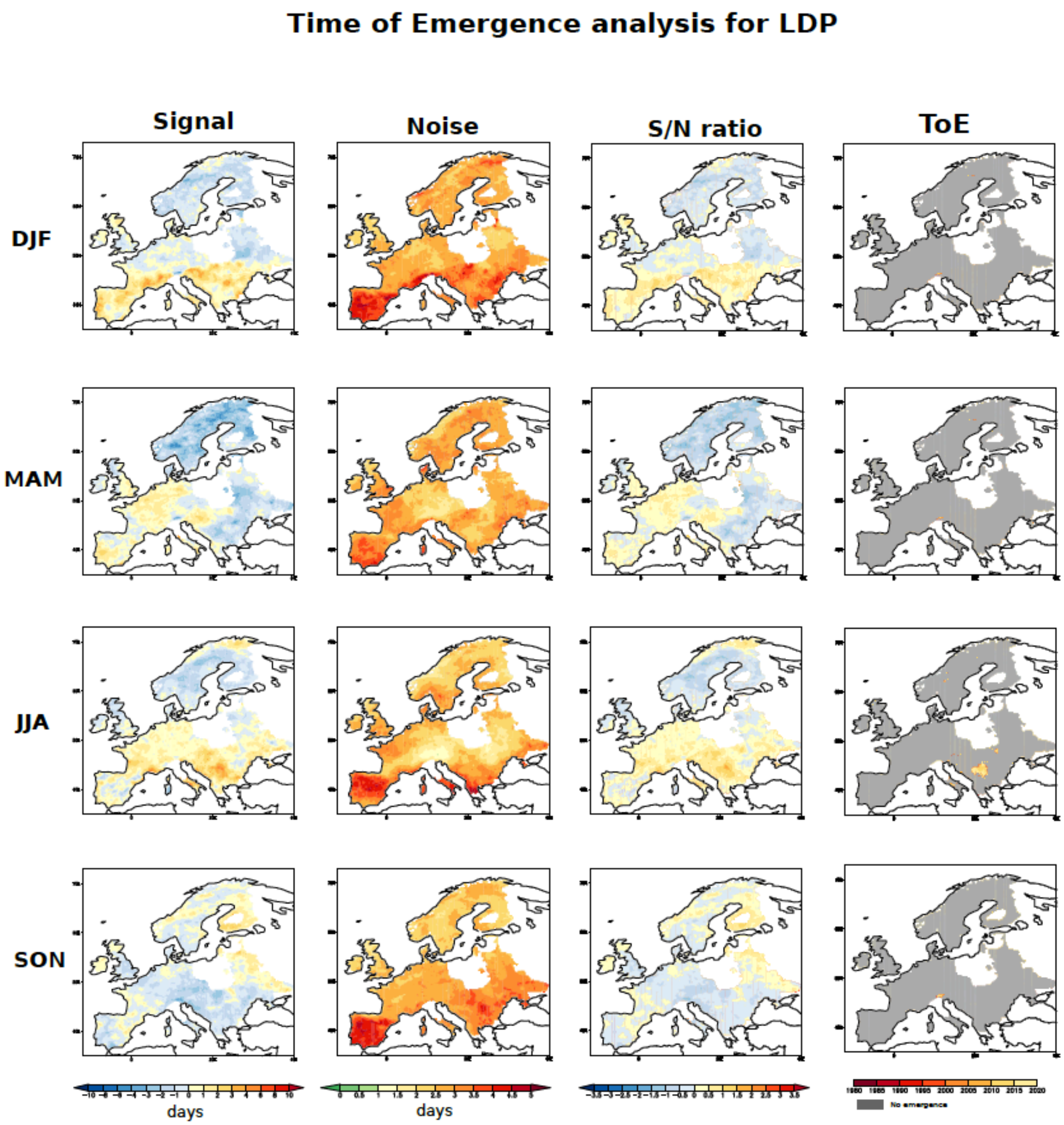

Figure 24: From left to right column: Signal, noise, signal-to-noise ratio and Time of Emergence (see section 3,2 for details on the calculation).

4. Summary

We have analysed the climatology, variability, tendency and Time of Emergence of a sub set of INDECIS-ISD. Below we summarise the main findings.

- The most significant TP changes are observed during wintertime when the climatological wet areas of northern Europe are becoming wetter (e.g., TP has increased 2.6%/decade over Scandinavia and 4.2%/decade over the British Isles), and the dry areas of southern Europe, especially the Iberian Peninsula (-2%/decade) are getting drier. A strong wetting trend is also observed over the Oriental Alps. In summer, the spatial pattern of TP tendencies is similar to winter, but their magnitude is weaker. Finally, during the transition seasons of autumn and spring, there is widespread wetting over Europe, although the trends are generally weak.
- The fraction of total precipitation due to very strong precipitation days has generally increased all over Europe in each season.
- During winter and springtime, LWP has increased over the UK, Scandinavia and N-E Europe and it has decreased over Central Europe and the Iberian Peninsula. Summer and autumn tendencies are very weak.
- Winter LDP tendencies exhibit a marked North-South dipole; LDP has increased over southern Europe and increase over northern Europe, especially over Scandinavia. During summer, LDP has increased over Continental Europe.
- An increase in the wet-day precipitation intensity is observed in many European regions throughout the year, whereas the wet-day frequency increases in the northeast of the continent in winter and decreases in scattered regions in all seasons.
- Temperature extremes (herein tropical nights and summer days) present an increasing and significant trend especially in the areas with the largest climatological values, whereas cold extremes (herein frost days and ice days) do not present statistically significant trends in the areas and seasons where the largest values occur.
- We have analysed the ToE for the indices TP, PVWD, LWP and LDP. Generally, the climate change signal has not emerged yet for any of these indices. An exception is TP over the oriental Alps, the signal of which has emerged after 2015 in all seasons.

- Vyver *et al.* (2019) (see Appendix 2) presents a piecewise linear quantile regression model technique to estimate the scaling parameters of extreme precipitation and test whether or not a pronounced super Clausius-Clapeyron scaling exists. The technique when applied to hourly station data across Western Europe and Scandinavia reveal large uncertainties in the scaling rates and show that the dew point temperature is a better scaling predictor than temperature.

5. References

Bedia, J., Herrera, S., Gutiérrez, J.M., Zavala, G., Urbieta, I.R., Moreno, J.M., 2012. Sensitivity of fire weather index to different reanalysis products in the Iberian Peninsula. Nat. Hazards Earth Syst. Sci. 12, 699–708. https://doi.org/10.5194/nhess-12-699-2012.

Casanueva, A., Rodríguez-Puebla, C., Frías, M. D., and González-Reviriego, N.: Variability of extreme precipitation over Europe and its relationships with teleconnection patterns, Hydrol. Earth Syst. Sci., 18, 709-725, https://doi.org/10.5194/hess-18-709-2014, 2014.

Hamed, K.H., Rao, A.R., 1998. A modified Mann-Kendall trend test for autocorrelated data. Journal of Hydrology 204, 182–196.

Hawkins, E., and Sutton, R. (2012), Time of emergence of climate signals, *Geophys. Res. Lett.*, 39, L01702, doi:10.1029/2011GL050087.

Mann, H.B., 1945. Nonparametric tests against trend. Econometrica 245–259.

Santer BD, Wigley TML, Boyle JS, Gaffen DJ, Hnilo JJ, Nychka D, Parker DE, Taylor KE (2000) Statistical significance of trends and trend differences in layer-average atmospheric temperature time series. J Geophys Res-Atmos 105:7337–7356.

Sen P. K.: Estimates of regression coefficient based on Kendalls Tau, J. Am. Stat. Assoc., 63, 1379–1389, doi:10.2307/2285891,1968.

Sheng, Y., Wang, C., 2004. The Mann-Kendall test modified by effective sample size to detect trend in serially correlated hydrological series. Water Resour. Manag. 201–218.

Sousa, P.M., Trigo, R.M., Aizpurua, P., Nieto, R., Gimeno, L., García-Herrera, R., 2011. Trends and extremes of drought indices throughout the 20th century in the Mediterranean. Natural Hazards and Earth System Sciences 33–51.

Van de Vyver, H., Van Schaeybroek, B., De Troch, R., Hamdi, R., Termonia, P. (2019) Modeling the scaling of short-duration precipitation extremes with temperature. *Earth Space Sci*. https://doi.org/10.1029/2019EA000665

Appendix 1: Precipitation based indices timeseries and trends

This appendix contains time series for TP, PVWD, LDP and LWP spatially averaged over the indicated geographical areas (Fig.A1) for the period 1950-2017. We included the linear trends.

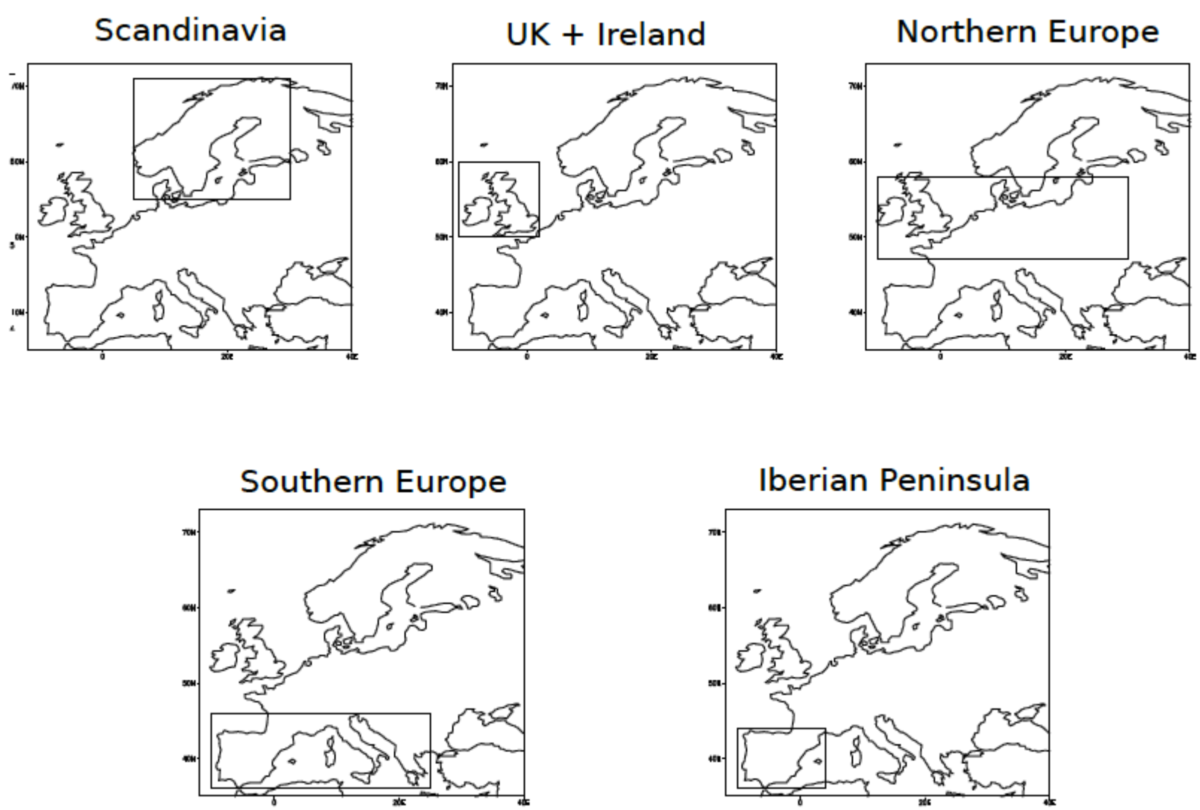

Figure A1: Designated geographical areas for which time series and tendencies are calculated.

Total precipitation time series and tendency (%/decade)

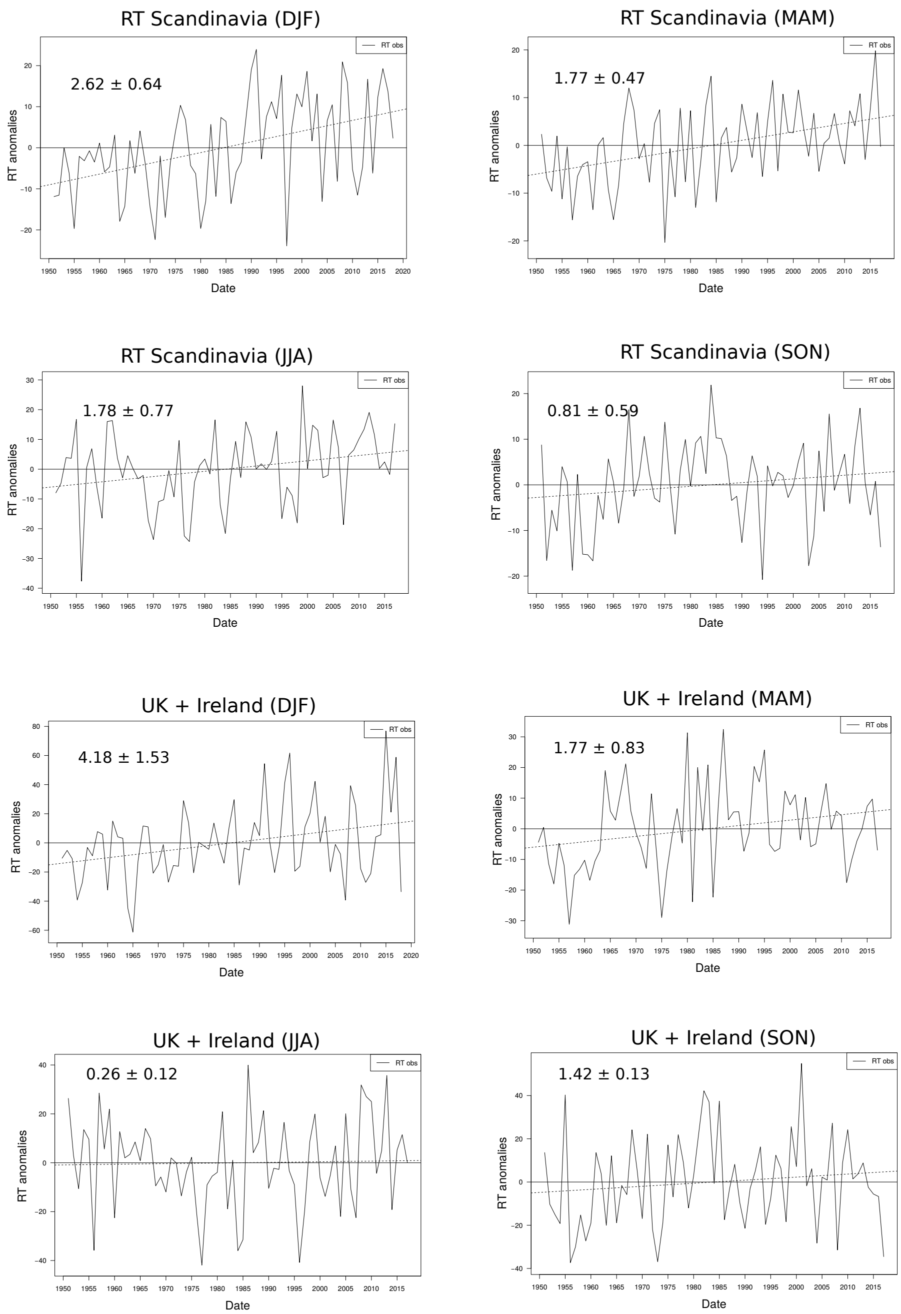

Figure A2: Observed TP anomalies (mm/month) spatially averaged over the indicated seasons and geographical regions and estimated linear trends for the period (1950-2017) expressed as a percentage of the climatology (%/decade). The standard error of the regression coefficient is also given.

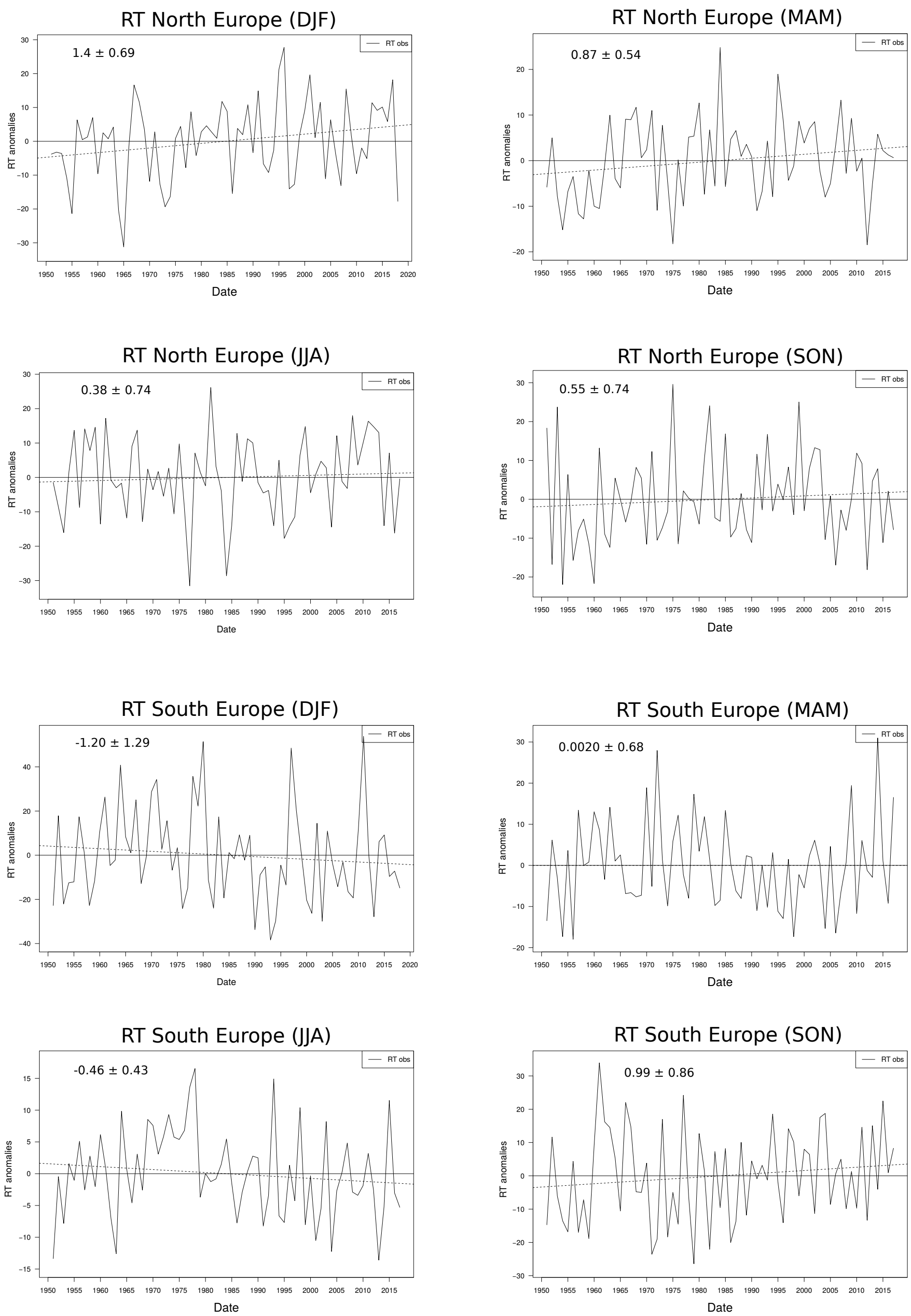

Figure A3: Observed TP anomalies (mm/month) spatially averaged over the indicated seasons and geographical regions, and estimated linear trends for the period (1950-2017) expressed as a percentage of the climatology (%/decade). The standard error of the regression coefficient is also given.

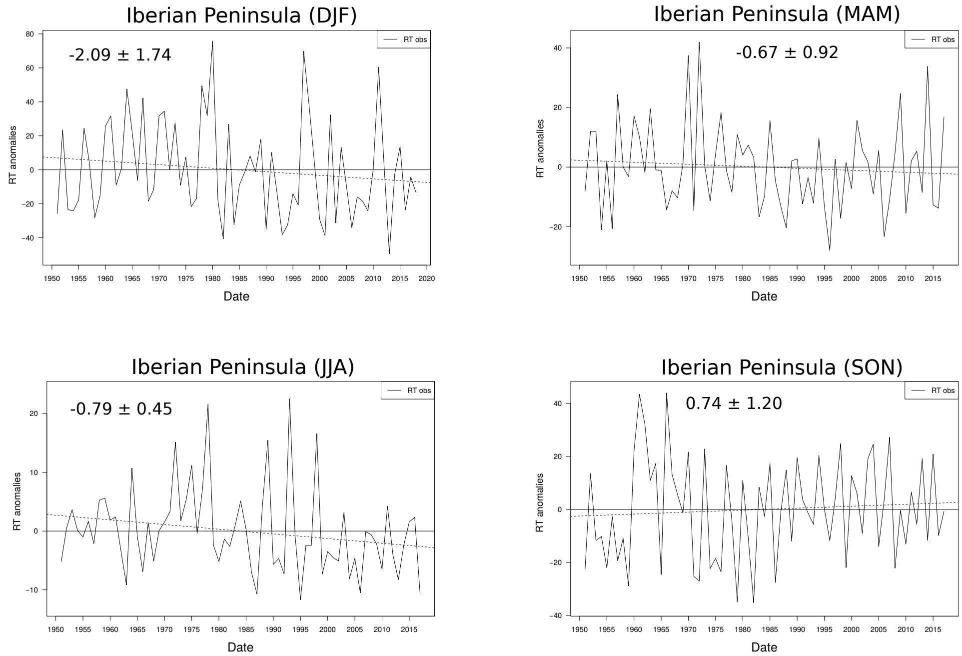

Figure A4: Observed TP anomalies (mm/month), spatially averaged over the indicated seasons and geographical regions, and estimated linear trends for the period (1950-2017) expressed as a percentage of the climatology (%/decade). The standard error of the regression coefficient is also given.

Fraction of the total precipitation due to very wet days and tendency (%/decade)

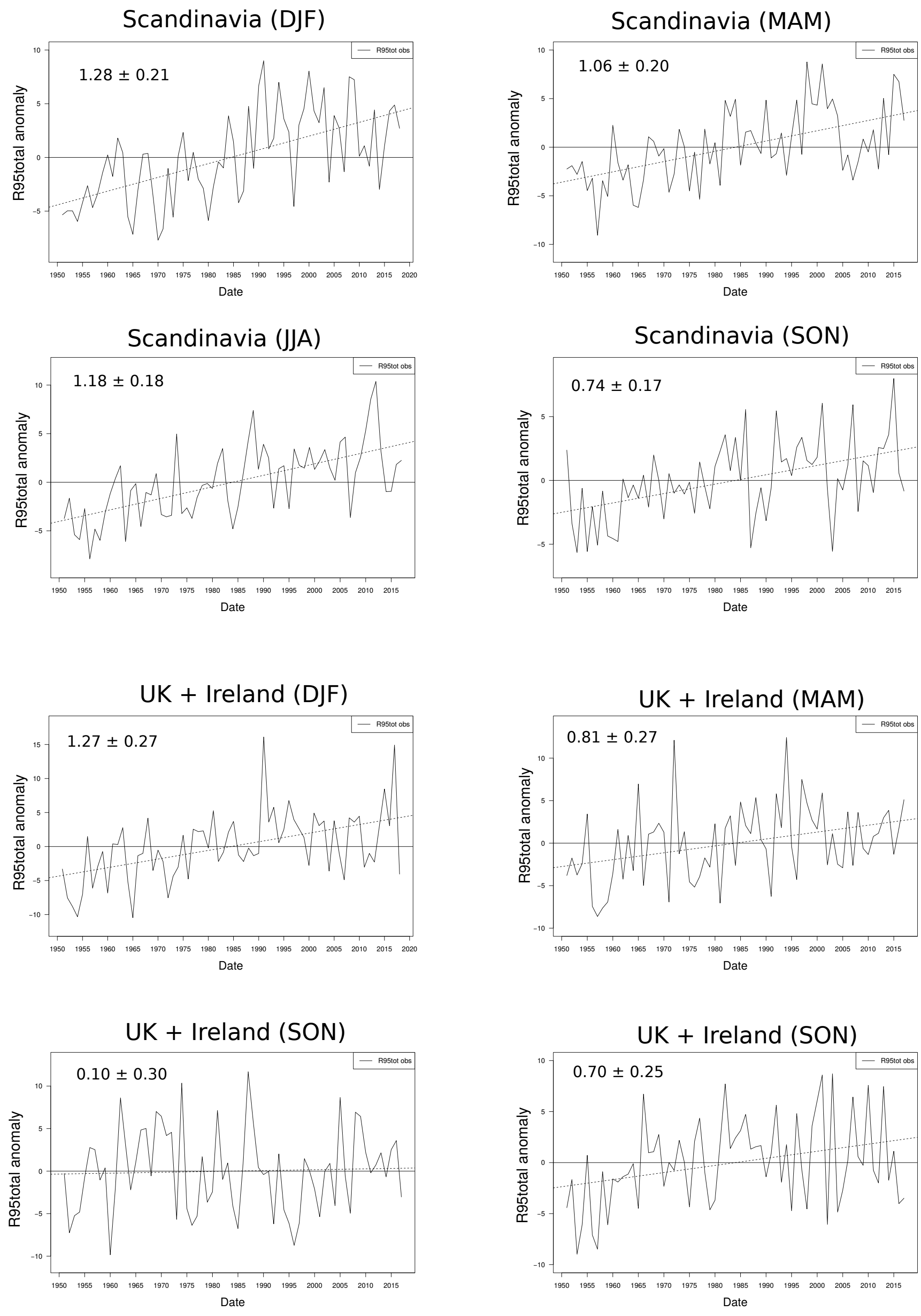

Figure A5: Observed PVWD anomalies (days), spatially averaged over the indicated seasons and geographical regions, and estimated linear trends for the period (1950-2017) expressed in PVWD units per decade (%/decade). The standard error of the regression coefficient is also given.

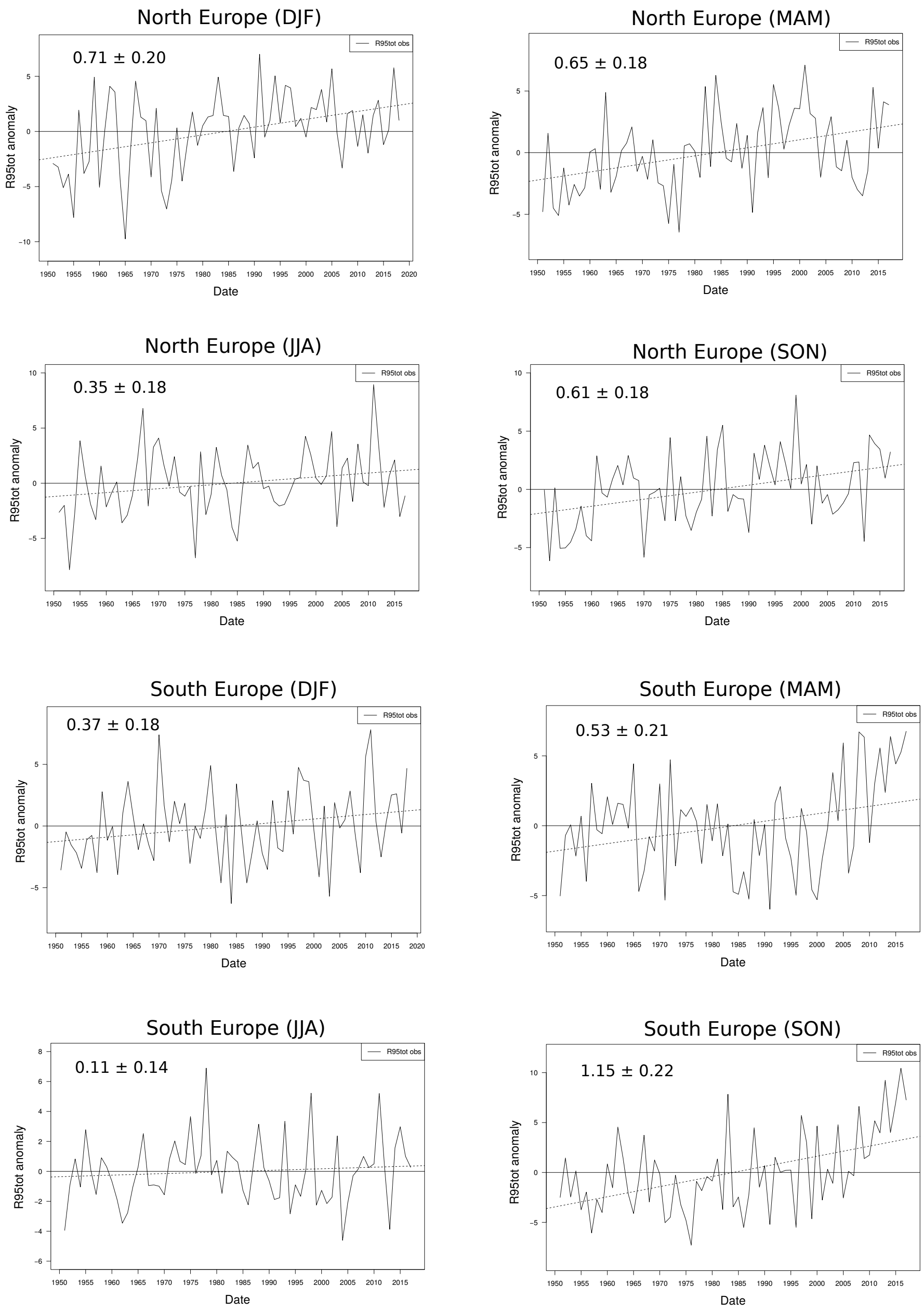

Figure A6: Observed PVWD anomalies (%) spatially averaged over the indicated seasons and geographical regions, and estimated linear trends for the period (1950-2017) expressed in PVWD units per decade (%/decade). The standard error of the regression coefficient is also given.

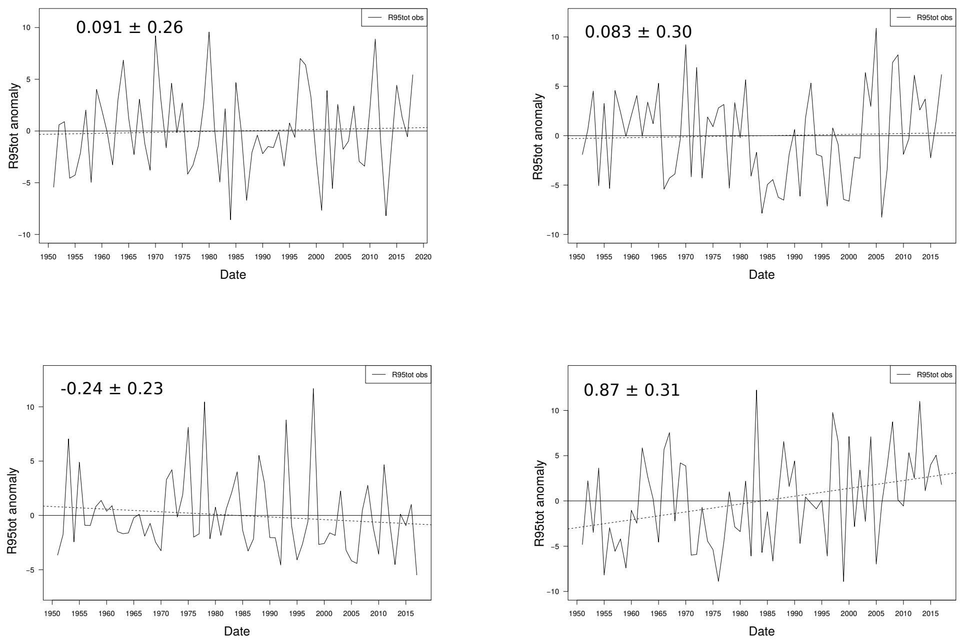

Figure A7: Observed PVWD anomalies (%) spatially averaged over the indicated seasons and geographical regions, and estimated linear trends for the period (1950-2017) expressed in PVWD units per decade (%/decade). The standard error of the regression coefficient is also given.

Longest Wet Period (LWP) time series and tendency (days/decade)

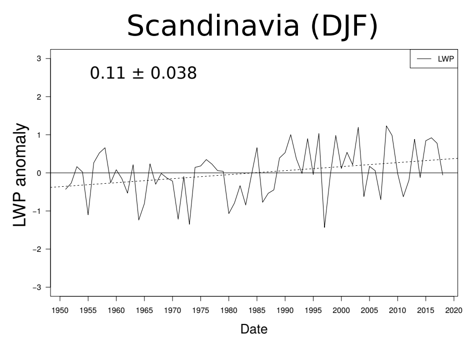

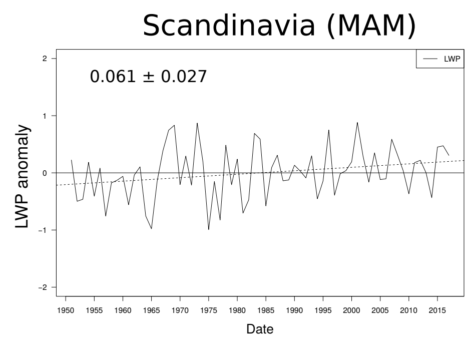

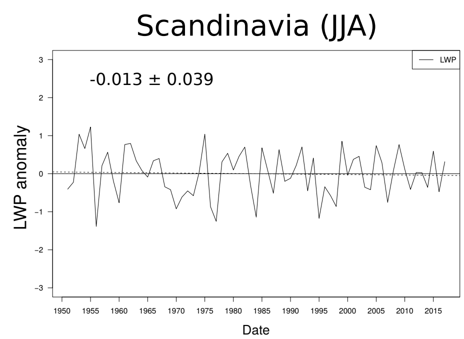

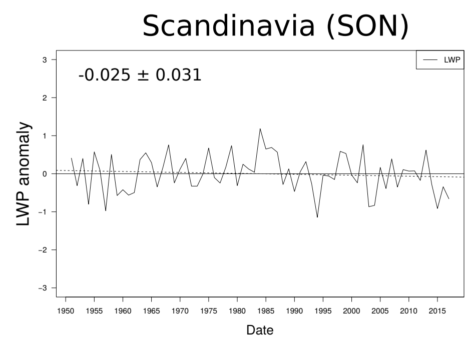

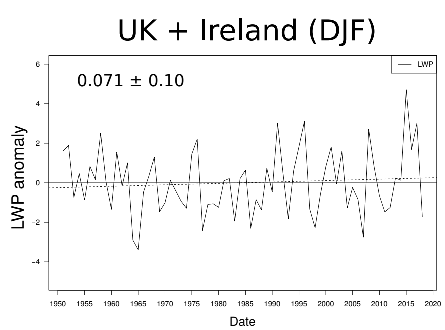

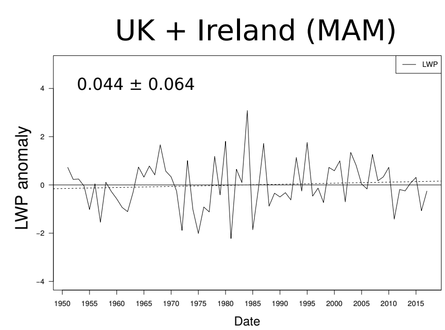

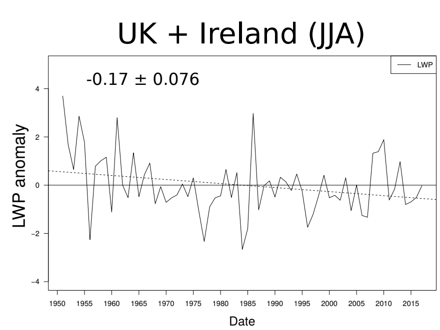

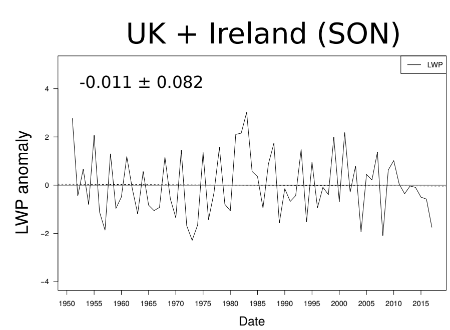

Figure A8: Observed LWD anomalies (days) spatially averaged over the indicated seasons and geographical regions, and estimated linear trends for the period (1950-2017) expressed in LWD units per decade (days/decade). The standard error of the regression coefficient is also given.

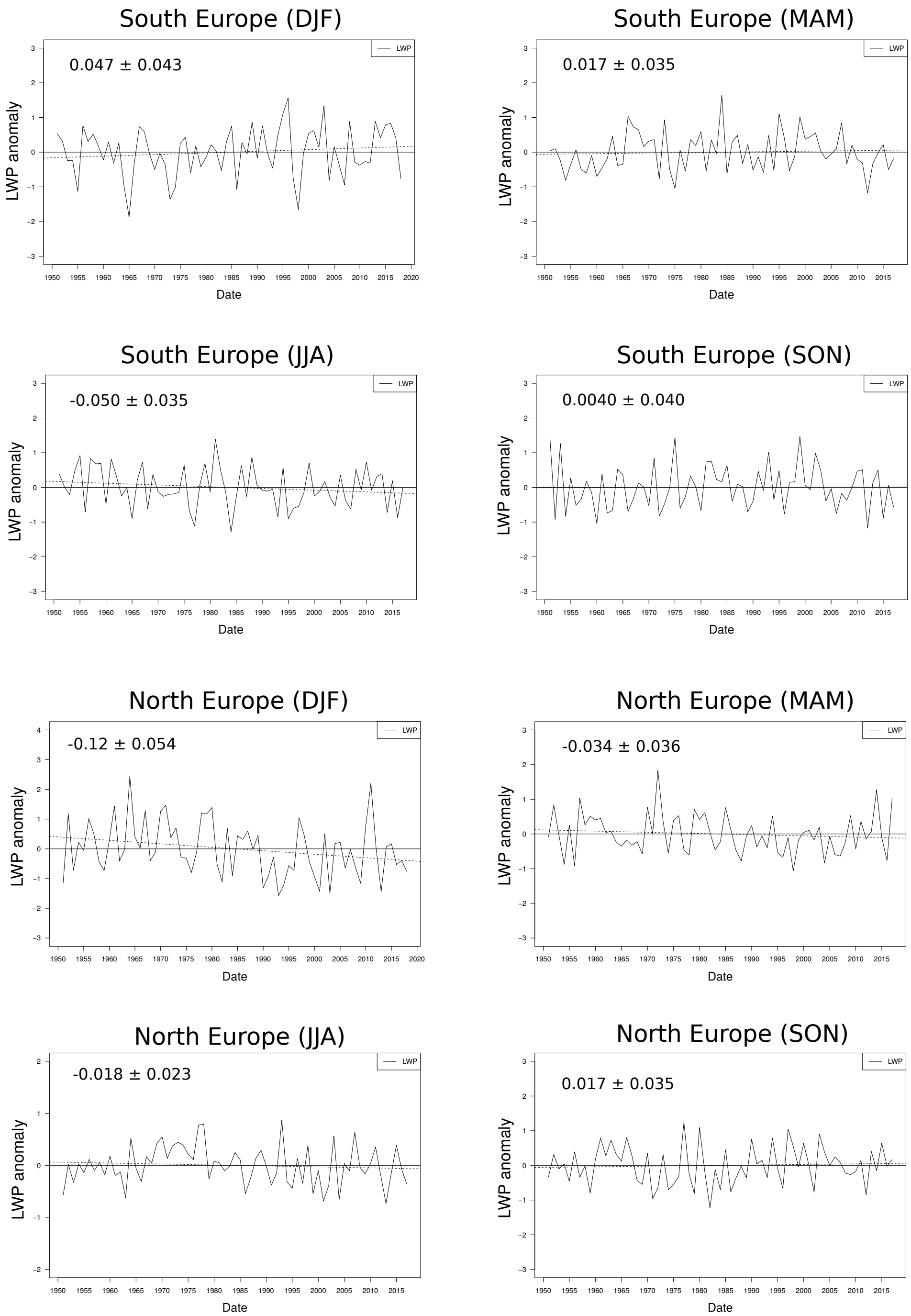

Figure A9: Observed LWD anomalies (days) spatially averaged over the indicated seasons and geographical regions, and estimated linear trends for the period (1950-2017) expressed in LWD units per decade (days/decade). The standard error of the regression coefficient is also given.

Longest dry period (LDP) timeseries and tendency (days/decade)

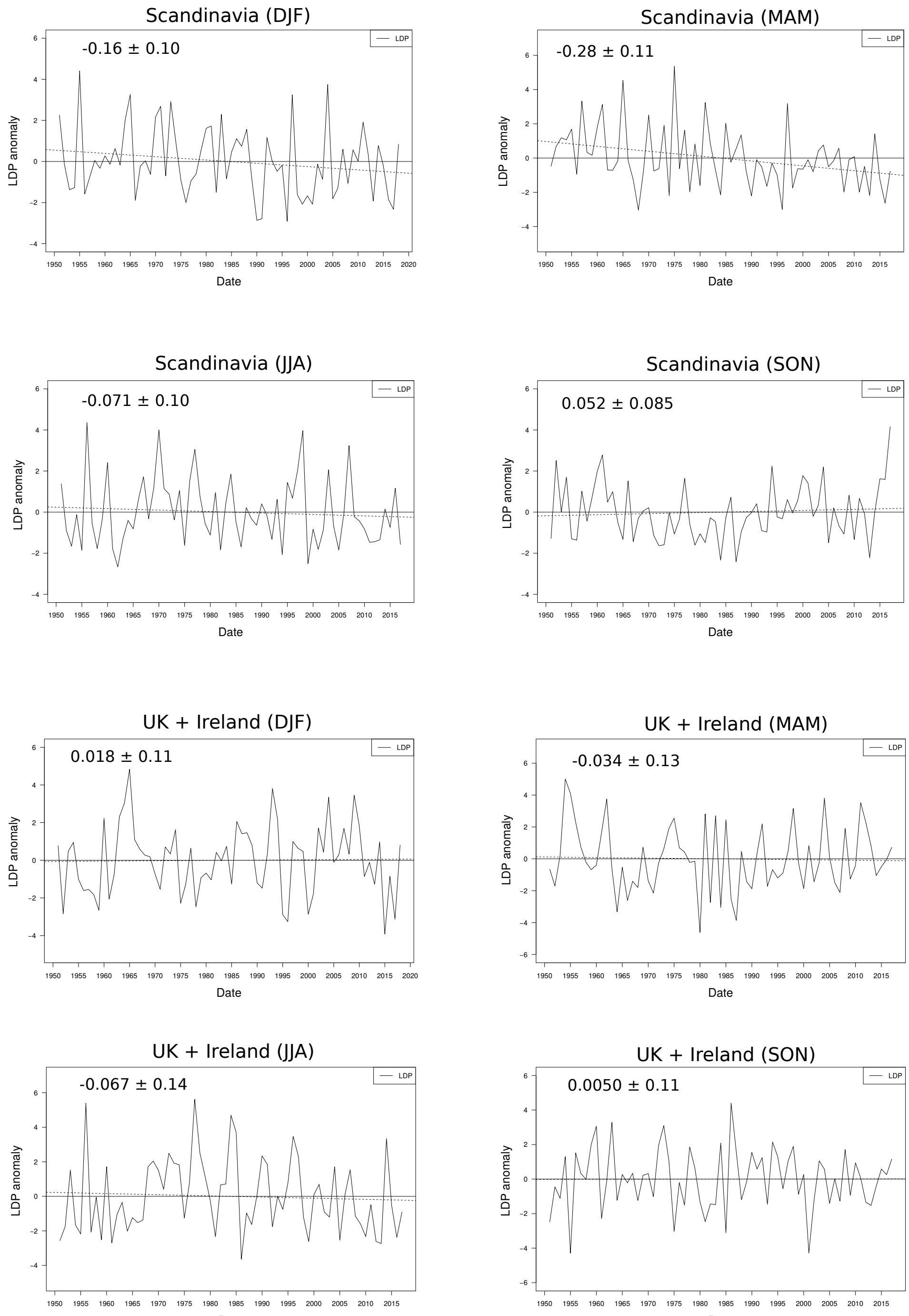

Figure A10: Observed LDP anomalies (days) spatially averaged over the indicated seasons and geographical regions, and estimated linear trends for the period (1950-2017) expressed in LDP units per decade (days/decade). The standard error of the regression coefficient is also given.

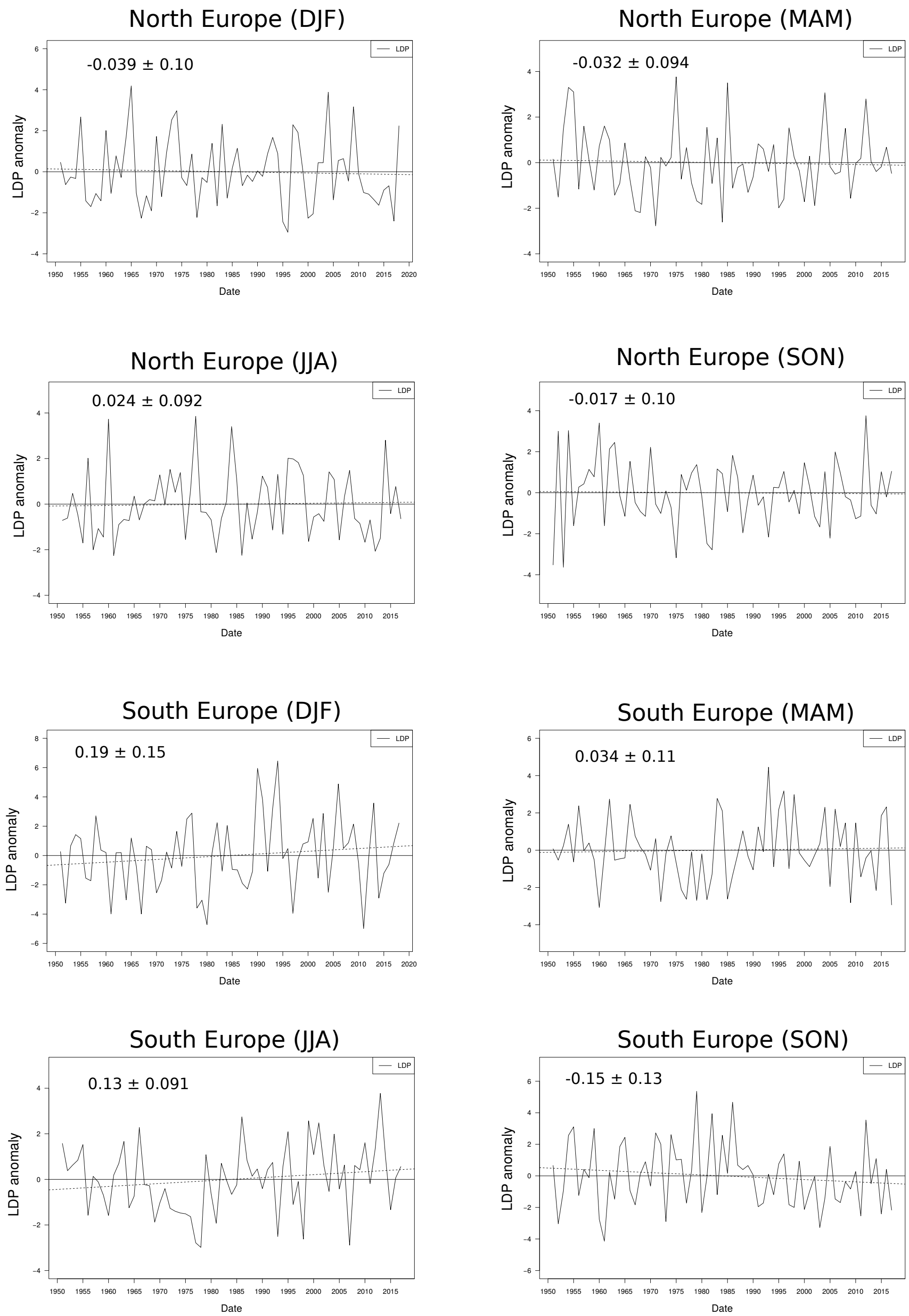

Figure A11: Observed LDP anomalies (days) spatially averaged over the indicated seasons and geographical regions, and estimated linear trends for the period (1950-2017) expressed in LDP units per decade (days/decade). The standard error of the regression coefficient is also given.

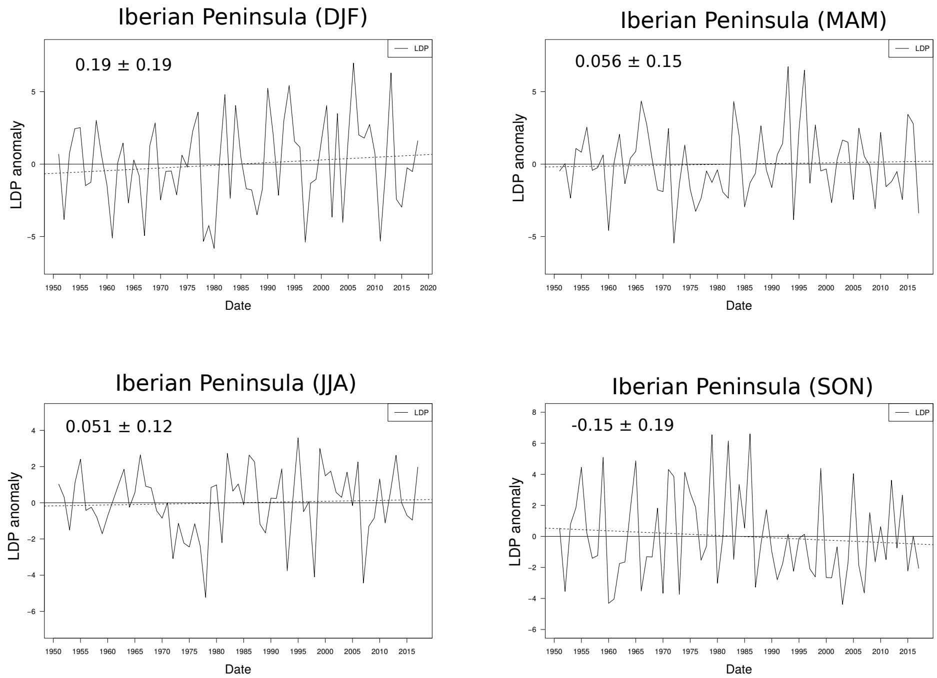

Figure A12: Observed LDP anomalies (days) spatially averaged over the indicated seasons and geographical regions, and estimated linear trends for the period (1950-2017) expressed in LDP units per decade (days/decade). The standard error of the regression coefficient is also given.

Appendix 2

RMI contribution to INDECIS D52

***Authors**: Hans Van de Vyver, Bert Van Schaeybroeck*

For more details, the reader is referred to Van de Vyver *et al.* (2019).

Introduction

The Clausius-Clapeyron (CC) relation expresses the exponential increase in the moisture holding capacity of air of approximately 7% per °C. Earlier studies show that extreme hourly precipitation increases with daily mean temperature, consistent with the Clausius-Clapeyron relation. Recent studies at specific locations found that for temperatures higher than around 12 °C, hourly precipitation extremes scale at rates higher than the CC-scaling, a phenomenon which is often referred to as *"super-CC scaling"*, see Lenderink and van Meijgaard (2008; 2010). These scalings are typically estimated by collecting rainfall data in temperature bins, followed by a linear fit or a visual inspection of the precipitation quantiles in each bin, see Fig. 1. In this study, a piecewise linear quantile regression model is presented for a more flexible, and robust estimation of the scaling parameters, and their associated uncertainties. Moreover, we use associated information criteria to prove statistically whether or not a pronounced super-CC scaling exists. The techniques were tested on stochastically simulated data, and, when applied to hourly station data across Western Europe and Scandinavia, revealed large uncertainties in the scaling rates. Finally, goodness-of-fit measures indicated that the dew point temperature is a better scaling predictor than temperature.

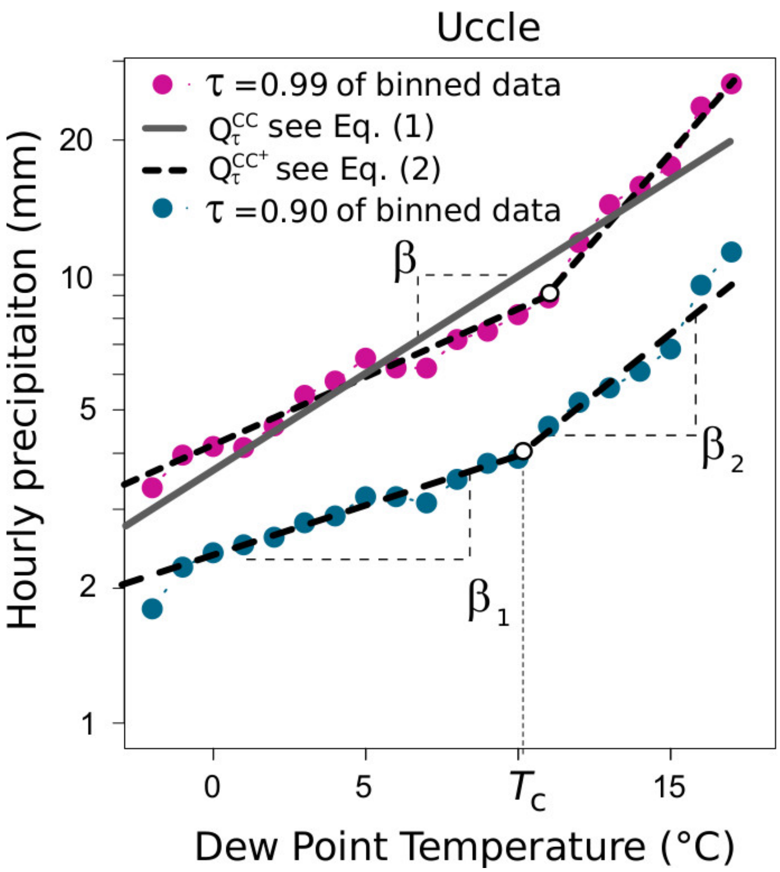

Fig. 1 *τ-quantiles of hourly precipitation as a function of the daily-mean dew temperature, for τ = 0.9 and τ = 0.99. Dotted lines: estimated with binning. Solid gray line: estimated with linear quantile regression. Black dashed line: estimated with piecewise linear quantile regression.*

Data and Methods

Long time quality-controlled series of hourly observed precipitation, temperature, and dew point temperature were collected for different locations in Western Europe and Scandinavia. These include Belgium (Uccle), The Netherlands (De Bilt), France (Paris, Lille, Toulouse, Lyon and Marseille), Germany (Nordrhein-Westfalen and Berlin), Sweden (Stockholm surrounding area, and Northern Sweden), and Finland (Helsinki). In the statistical analysis, neighboring station data were treated as one single dataset, as is commonly done to improve the estimation of extremes (Buishand, 1991; Hosking & Wallis, 1997; Davison *et al.*, 2012). As in the original approach of Lenderink and van Meijgaard (2010), we computed the daily-mean dew point temperature. Data points were excluded (i) when precipitation observations are equal to, or less than 0.1 mm, (ii) when hourly instantaneous temperatures are below 0 °C (to avoid snow), (iii) for events associated with the downturn in precipitation extremes (mostly dew point temperatures above 18 °C--20 °C), as this is likely due to a lack of moisture content, and (iv) when the daily mean temperature exceeds 24 °C because Hardwick-Jones *et al.* (2010) found a reduction in relative humidity in such a case, which may affect the scaling relationship. As in Wasko and Sharma (2014), rainfall events were separated by 5 h of no precipitation, and we withheld the maximum precipitation depth within each event.

Wasko and Sharma (2014) have shown that, in case of a constant scaling across a wide temperature range, the use of linear quantile regression (Koenker, 2005) is superior to the binning approach for extracting the scaling properties. In particular, the quantile regression estimator is asymptotically unbiased (Koenker & Basset, 1978), in contrast to the binning approach. Moreover, a proper statistical framework is necessary given the lack of long and reliable sub-daily time series (Westra *et al.*, 2014; Li *et al.*, 2019). For locations exhibiting super-CC scaling, applying an additional piecewise linear quantile regression to both ranges ($T > T$c and Tc $< T <$ 19 °C, with $T_{c,}$ the *change-point*) turns out to be problematic: first, if the change point is not known in advance, the regression lines may show a discontinuity at the change point. Second, linear quantile regression provides uncertainty estimates of the scaling rates, but the uncertainty in the change-point cannot be obtained.

We applied the piecewise linear quantile regression framework of Li *et al.* (2011) by simultaneously estimating the scaling rates and the change point. In Fig. 1, the quantiles (dashed lines) provided by the change-point model of Li *et al.* (2011) have been added, which is made up of two different lines with slopes β_1 and β_2 instead of a single slope β. The work of Wasko and Sharma (2014) is extended here in the sense that we model two scaling regimes and, in addition, propose a more complete inference, including uncertainty estimation, model selection with information criteria, and predictor selection with goodness-of-fit measures. In what follows, we denote by CC and CC+, the linear- and piecewise linear quantile regression model, respectively.

Results

The application of the quantile regression models to the observational time series is demonstrated in Fig. 2. Based on the BIC values for the 0.9-quantile (not shown), the CC+ model is better than the CC model for Uccle, De Bilt, Nordrhein-Westfalen, Berlin, Lille, Paris, Toulouse and Marseille. For the remaining locations (e.g. Lyon, Stockholm surrounding area, Northern Sweden and Helsinki), the lowest BIC values at the 0.9-quantile, were obtained by the CC model.

Fig. 3 shows the inference results for all the locations where the CC+ model is significant, for the particular choice $\tau = 0.99$. The confidence intervals of β_1 (Fig. 3a) cover the range 5-10% per °C, and are thus compatible with the well-known CC-rate of 7% per °C. The estimation of the super-CC scaling rate in De Bilt (around 14% per °C) agrees well with the results shown in Fig. 2c of Lenderink and van Meijgaard (2010), giving extra confidence to our results. Most likely, the scaling rates seem to change by a factor of more than two (Fig. 3c) although, due to the large estimation uncertainties, assessing potential regional differences in the scaling rates is difficult. Confidence intervals for Lille and Marseille are particularly large, but the estimation was based on less than 10000 data pairs.

The scaling was tested for different predictors by means of the goodness-of-fit criterion. As potential candidate predictors, the temperature and the dew point temperature were compared (Fig. 4). The predictive skill of the dew point temperature is slightly, but systematically higher than that of the temperature, which is physically plausible. Note also that, irrespective of the predictor, the predictive skill at locations with a change point is significantly higher than at locations with no change point (Scandinavian stations and Lyon).

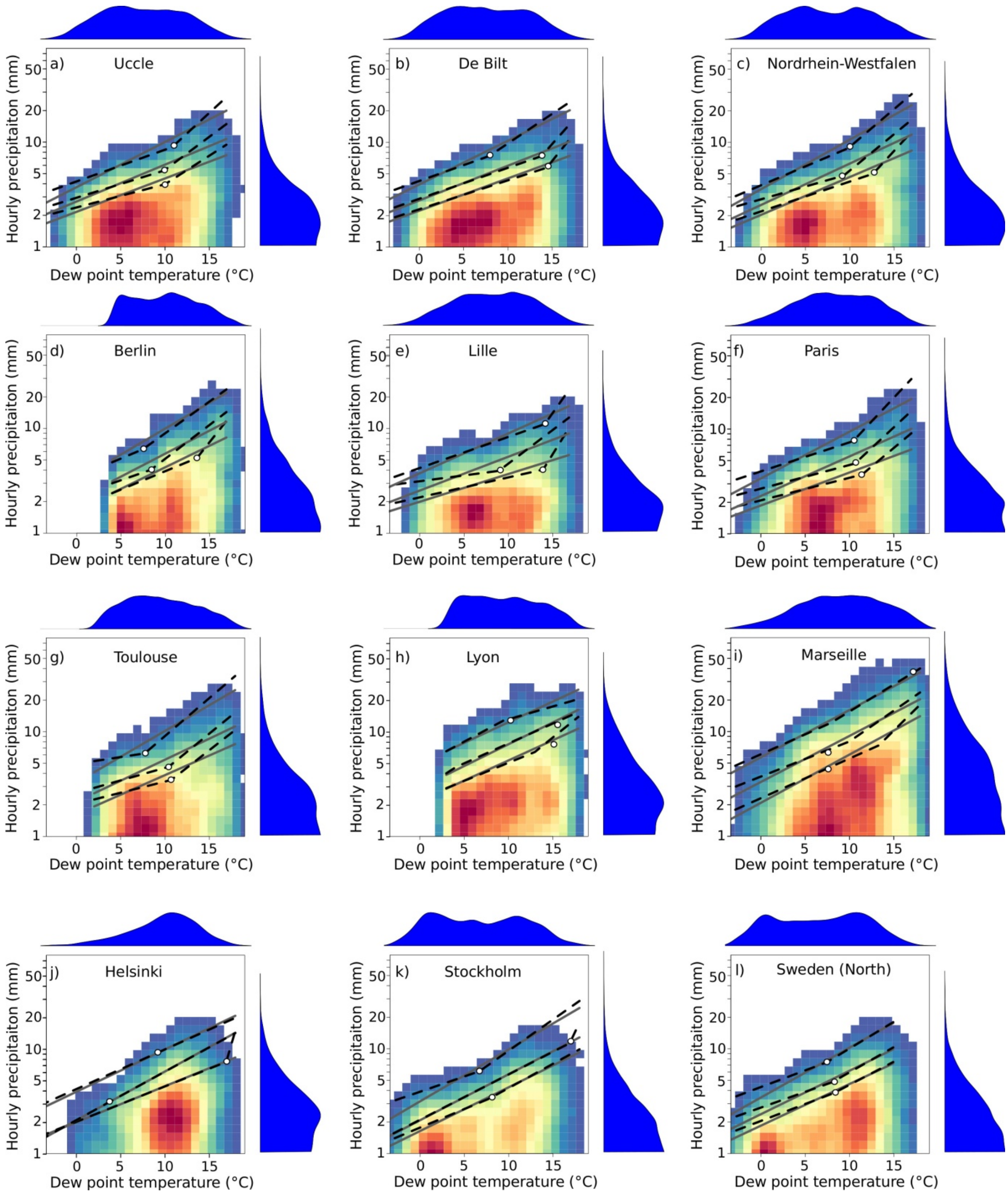

Fig. 2 *τ -quantile estimates of hourly precipitation (mm), with τ = 0.90; 0.95; 0.99. <u>Solid lines</u>: linear quantile regression lines (CC). <u>Dashed lines</u>: piecewise linear quantiles regression lines (CC+). The shaded areas represent the two-dimensional histogram. The probability distribution of log P (right bar) is truncated at P = 1.*

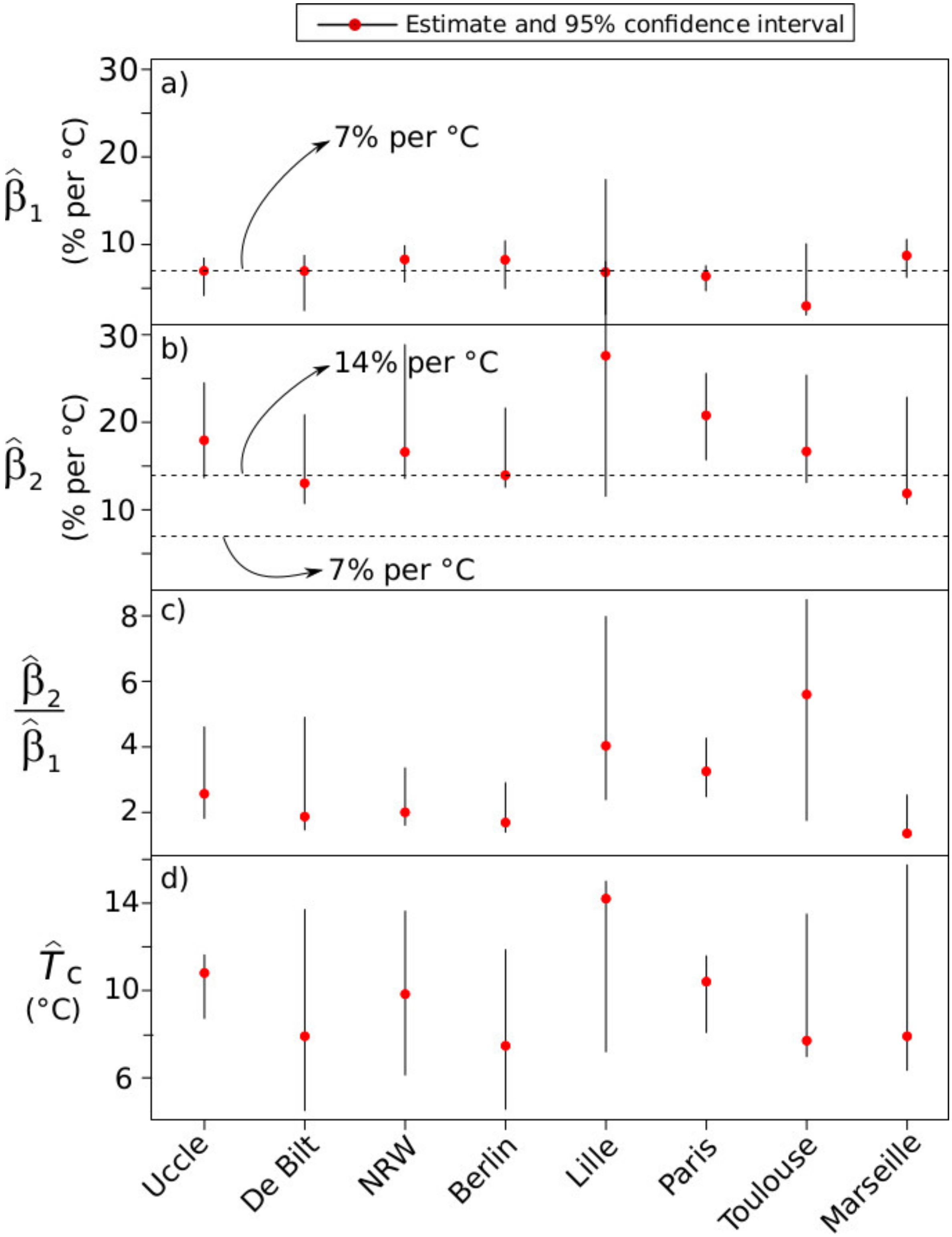

Fig. 3 *Inference results for the CC+ model, for different locations, and τ = 0.99. (NRW: Nordrhein-Westfalen).*

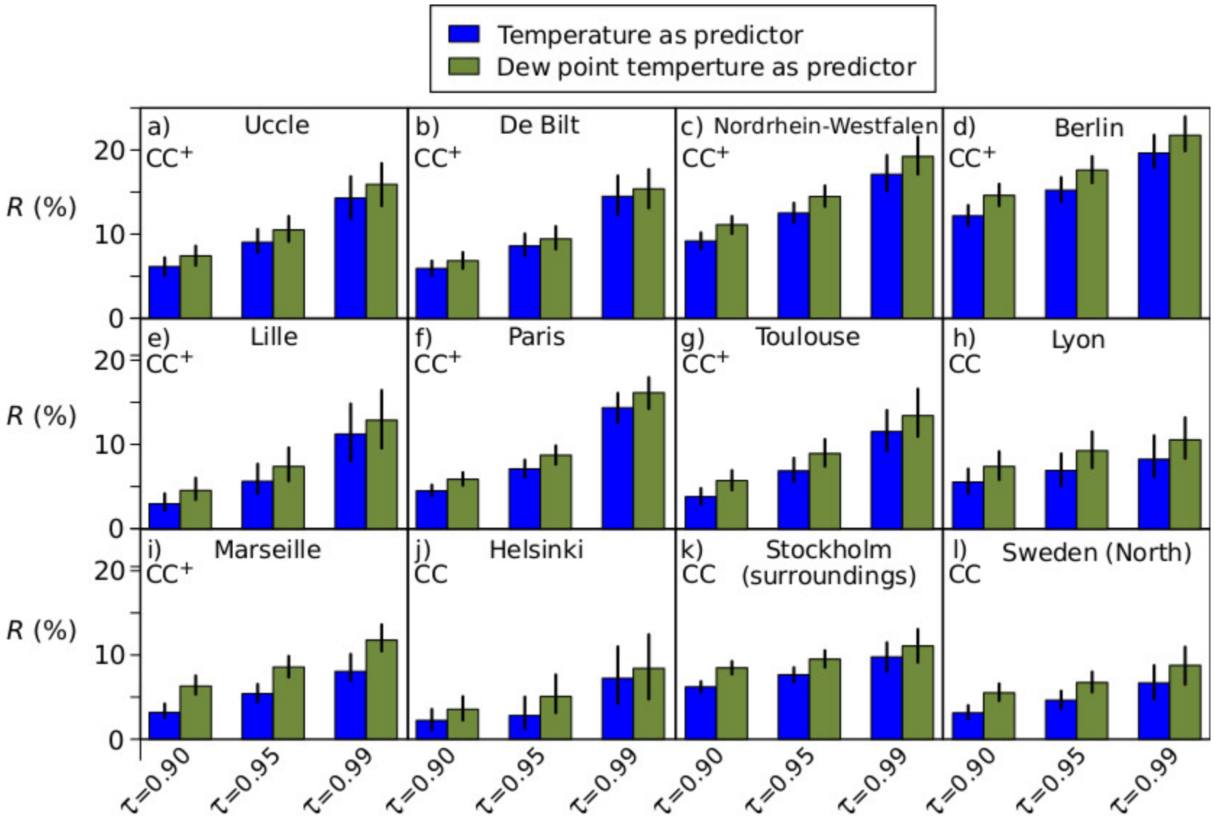

Fig.4 *The goodness-of-fit criterion. For each station, the BIC-selected model was considered (either CC or CC+). The vertical lines indicate the 95 % confidence intervals of R (i.e. the goodness-of-fit criterion).*

Conclusions and outlook

It was found that:

1. Simulations with simple stochastic models showed that, for a realistic sample size of n = 10^4, the estimator is fairly unbiased and has a reasonable uncertainty, unless i) the scaling rates differ only slightly, and to a lesser extent ii) the change-point temperature is at the upper percentiles of it's distribution.
2. Simulations with simple stochastic models showed that BIC-based inference is useful in detecting the existence of a change point. However, when there is no change point, the success rate at the 0.9-quantile is acceptable, but decreases at increasing quantiles.

3. The results show a strong evidence for the change-point model in Western Europe. Results at Marseille suggest also a change point, but the change in the scaling rates is smaller than for Western Europe. On the contrary, evidence lacks for the change point model in the Scandinavian stations and in Lyon.
4. Although deviations from linear scaling are evidenced at multiple locations, the associated estimations for change points and scaling rates are highly uncertain. More specifically, the factorial change in the scaling coefficients ranges between 2 and 5, while the change-point estimates ranges between 5 °C and 15 °C.

5. In view of the recent controversy regarding using air temperature/dew point temperature as proxies for extreme precipitation, an approach is presented to discriminate the best predictor. More specifically, at all observational locations, dew point temperature is slightly superior to temperature as a predictor for extreme precipitation. Moreover, locations with a change point show larger overall explanatory skill than locations without a change point.

References

Buishand, T. (1991). Extreme rainfall estimation by combining data from several sites. *Hydrolog. Sci. J.*, 36 (4), 345--365.

Davison, A. C., Padoan, S. A., & Ribatet, M. (2012). Statistical modeling of spatial extremes. *Statist. Sci.*, 27 (2), 161--186.

Hardwick-Jones, R., Westra, S., & Sharma, A. (2010). Observed relationships between extreme sub-daily precipitation, surface temperature, and relative humidity. *Geophys. Res. Lett.*, 37 (22), L22805.

Hosking, J. R. M., & Wallis, J. R. (1997). *Regional Frequency Analysis: An Approach Based on L-Moments*. Cambridge University Press.

Koenker, R. (2005). *Quantile regression*. Cambridge University Press, Cambridge.

Koenker, R., & Basset, G. (1978). Regression quantiles. *Econometrica*, 46 (1), 33--55.

Lenderink, G., & van Meijgaard, E. (2008). Increase in hourly extreme precipitation beyond expectations from temperature changes. *Nat. Geosci.*, 1 , 511--514.

Lenderink, G., & van Meijgaard, E. (2010). Linking increases in hourly precipitation extremes to atmospheric temperature and moisture changes. *Environ Res. Lett.*, 5 , 025208.

Li, C., Wei, Y., Chappell, R., & He, X. (2011). Bent line quantile regression with application to an allometric study of land mammals' speed and mass. *Biometrics*, 67 (1), 242-249.

Li, C., Zwiers, F., Zhang, X., & Li, G. (2019). How much information is required to well constrain local estimates of future precipitation extremes? *Earths Future*, 7 (1), 11--24.

Van de Vyver, H., Van Schaeybroek, B., De Troch, R., Hamdi, R., Termonia, P. (2019) Modeling the scaling of short-duration precipitation extremes with temperature. *Earth Space Sci*. https://doi.org/10.1029/2019EA000665

Wasko, C., & Sharma, A. (2014). Quantile regression for investigating scaling of extreme precipitation with temperature. *Water Resour. Res.*, 50 (4), 3608--3614.

Westra, S., Fowler, H., Evans, J., Alexander, L., Berg, P., Johnson, F., . . . Roberts, N. (2014). Future changes to the intensity and frequency of short-duration extreme rainfall. *Rev. Geophys.*, 52 , 522--555.

Appendix 3

On the use of satellite data to assess precipitation trends in Italy

1. Overview

One of the most important ways to assess climate change is to clearly establish statistically meaningful changes to mean values of a series of variables, the most important and widely used among whom are precipitation and temperature.

In order to establish trends over a region, in recent years there has been a growth in the importance and use of satellite data to complete information coming from weather stations and on-ground measurements of various kind. This is especially relevant not only for areas where on-ground measurement networks are sparse and not adequate to resolve meteorological phenomena, but also because satellite products are regular in space and time, making it interesting to compare them even with regularly gridded reanalysis products.

In this study, TRMM satellite data, with full years of daily data available from 1998 to 2018 included, were used as an example to assess the presence of trends of precipitation over Italy with the Mann-Kendall method.

Validation studies were carried out to establish the reliability of TRMM data in measuring precipitation and its features (e.g., Adler et al., 2002; Kästner and Steinwagner, 2004; Li et al., 2019). Thus, TRMM precipitation was used to determine SPI or precipitation trends (e.g., De Jesús et al., 2016; Levina et al., 2016). TRMM precipitation data have also been used successfully in several meteorological and climatological studies in the Mediterranean area (e.g., Mehta and Yang, 2008; Gabella et al., 2011; Kalimeris and Kolios, 2019).

2. Methodology

In this application TRMM daily data available from 01/01/1998 to 31/12/2018 were used at an approximately 25 km spaced grid. For the purpose of our study, we summed daily data into monthly cumulated precipitation.

The well-known Mann-Kendall test has been applied to assess the presence of a monotonic upward or downward trend (Mann, 1945; Kendall, 1979; Gilbert, 1987). In particular, statistical significance was assessed by means of a confidence levels $\alpha = 10$.

3. Results

Figures 1-3 show the grid points with an increase (blue) and decrease (red) in precipitation according to the Mann-Kendall analysis. TRMM satellite data do not show significant trends for yearly precipitation for most of Italy, except for an increase in precipitation for a few grid points in Calabria (southern Italy) and a decrease in Abruzzo (Adriatic coast of central Italy). However, results on both seasonal and monthly scale showed clear changes in the distribution patterns of precipitation over the country.

For winter, while there is a clear negative trend in central-eastern Italy, and a precipitation increase over northern Tuscany and, more sketchily, in northern Italy, monthly trends show a clear shift of precipitation distribution from December to February.
A similar shift occurs in spring: most of Italy experiences a reduction in precipitation in April, while March precipitation increases in many areas of the country.
In autumn, north-western Italy (roughly the regions of Piedmont, Lombardy and Liguria) and Abruzzo show a decline in precipitation, mainly occurring in September, while in the south various areas experience a positive precipitation trend: northern Puglia especially in September, Sicily in October and Calabria in November.
Comparing the seasonal and monthly maps to the yearly map, we can explain the negative trend of Abruzzo and southern Marche in central-eastern Italy as they are the only areas of the country that suffer both a negative trend in spring (April) and autumn-winter (September, December), but at the same time they do not benefit from the February and March increases which are experienced in most of Italy.
These results only partially confirm past studies on the Mediterranean basin which evidenced negative trends for annual and winter precipitation (De Luis et al. 2000; Xoplaki et al. 2006; Feidas et al. 2007; del Rio et al. 2010; Caloiero et al. 2018). As regards Italy, this trend behavior has been detected, in particular, in some areas of southern Italian regions, as in the case of Campania (Diodato 2007; Longobardi and Villani 2010), Basilicata (Piccarreta et al. 2004), Calabria (Caloiero et al. 2011, 2015, 2016; Brunetti et al. 2012), Sicily (Cannarozzo et al. 2006; Liuzzo et al. 2016) and Sardinia (Montaldo and Sarigu 2017; Caloiero et al. 2019). The different trend behavior between this work and past studies can be due to the length of the rainfall series, in fact, the decreasing winter precipitation mostly started in the 1970s and proceeded with an accumulation of dry years in the 1980s and 1990s (e.g. Piervitali et al. 1997; Schonwiese and Rapp 1997).

4. Conclusions

It's clear that the trend in precipitation shown by Mann-Kendall analysis performed on TRMM data, if really confirmed, can bring dramatic consequences to vegetation, agriculture and to the tourism industry, especially on winter tourism.
Two areas are particularly hit in this respect. The loss of precipitation in September in north-western Italy impacts the whole of the Po river hydrological basin, as the replenishing of water to the basin after the summer can have grave consequences on agricultural activities, and on water availability for domestic and industrial use.
At the same time, the shift in precipitation from December to February will have an impact on winter tourism on the Apennines mountain change, especially in a region like Abruzzo that has a thriving skiing activity.
Aside from the meaningful results for this test study, it is evident that the use of Mann-Kendall trend analysis for gridded data can be of major importance to highlight vulnerable areas in a country. This will allow not only to locate areas that might need

additional climatological studies, but also political interventions and favour the design and agenda of meeting between scientists and local stakeholders to tackle problems.
In order to better appreciate the results of this study, it is of major relevance to note that we considered only 21 years of data, as this is the TRMM time availability, but the recommended time for climatological analysis is to take into account at least 30 years of data when possible.

Bibliography

- Adler, R.F.; Huffman G.; Bolvin D.: **TRMM and GPCP initial cross-comparison**, GEWEX News, 12 (Nov): 5-6, 2002.
- Brunetti M.; Caloiero T.; Coscarelli R.; Gullà G.; Nanni T.; Simolo C.: **Precipitation variability and change in the Calabria region (Italy) from a high resolution daily dataset**, International Journal of Climatology, 32, 55-73, 2012.
- Caloiero T.; Coscarelli R.; Ferrari E., Mancini M.: **Trend detection of annual and seasonal rainfall in Calabria (southern Italy)**, International Journal of Climatology, 31, 44-56, 2011.
- Caloiero T.; Buttafuoco G.; Coscarelli R.; Ferrari E.: **Spatial and temporal characterization of climate at regional scale using homogeneous monthly precipitation and air temperature data: an application in Calabria (southern Italy)**, Hydrology Research, 46, 629-646, 2015.
- Caloiero T.; Callegari G.; Cantasano N.; Coletta V.; Pellicone G.; Veltri A.: **Bioclimatic analysis in a region of southern Italy (Calabria)**. Plant Biosystems, 150, 1282-1295, 2016.
- Caloiero T.; Caloiero P.; Frustaci F.: **Long-term precipitation trend analysis in Europe and in the Mediterranean basin**, Water and Environment Journal, 32, 433-445, 2018.
- Caloiero T.; Coscarelli R.; Gaudio R.; Leonardo G.P.: **Precipitation trend and concentration in the Sardinia region**, Theoretical and Applied Climatology, 137, 297-307, 2019.
- Cannarozzo M.; Noto L.; Viola F.: **Spatial distribution of rainfall trends in Sicily (1921–2000)**, Physics and Chemistry of the Earth, 31, 1201-1211, 2006.
- De Jesus A.; Brena-Naranjo J.A.; Pedrozo-Acuna A.; Yamanaka V.H.A.: **The Use of TRMM 3B42 Product for Drought Monitoring in Mexico**, Water, 8, 18, 2016.
- De Luis M.; Raventos J.; Gonzalez-Hidalgo J.C.; Sanchez J.R.; Cortina J.: **Spatial analysis of rainfall trends in the region of Valencia (East of Spain)**, International Journal of Climatology, 20, 1451-1469, 2000.
- del Rio S.; Herrero L.; Fraile R.; Penas A.P.: **Spatial Distribution of Recent Rainfall Trends in Spain (1961–2006)**, International Journal of Climatology, 31, 656-667, 2011.

- Diodato N.: **Climatic fluctuations in Southern Italy since 17th century: reconstruction with precipitation records at Benevento**. Climatic Change, 80, 411-431, 2007.
- Feidas H.; Noulopoulou Ch.; Makrogiannis T.; Bora-Senta E.: **Trend analysis of precipitation time series in Greece and their relationship with circulation using surface and satellite data: 1955–2001**. Theoretical and Applied Climatology, 87, 155-177, 2007.
- Gabella M.; Morin, E.; Notarpietro, R.: **Using TRMM spaceborn radar as a reference for compensating ground-based radar range degradation: Methodolog verification based on rain gauges in Israel**, Journal of Geophysical Research, 116, D02114, 2011.
- Gilbert, R.O.: **Statistical Methods for Environmental Pollution Monitoring**, Wiley, NY, 1987.
- Kalimeris, A., and Kolios, S.: **TRMM-based rainfall variability over the Central Mediterranean and its relationships with atmospheric and oceanic climatic modes**, Atmospheric Research, 230, 2019 .
- Kendall, M.G. **Rank Correlation Methods**, 4th edition, Charles Griffin, London, 1975.
- Kästner M., and Steinwagner, J. P**recipitation in the mediterranean region observed with trmm microwave data**, 2004.
- Levina; Hatmoko, W.; Seizarwati, W.; Vernimmen, R.: **Comparison of TRMM Satellite Rainfall and APHRODITE for Drought Analysis in the Pemali-comal River Basin**, Procedia Environmental Sciences, 33, 187-195, 2016.
- Li, N.; Wang, Z.; Chen, X.; Austin, G.: **Studies of General Precipitation Features with TRMM PR Data: An Extensive Overview**, Remote Sensing, 11, 80, 2019.
- Liuzzo L.; Bono E.; Sammartano V.; Freni G.: **Analysis of spatial and temporal rainfall trends in Sicily during the 1921–2012 period**, Theoretical and Applied Climatology, 126, 113-129, 2016.
- Longobardi A.; Villani P.: **Trend Analysis of Annual and Seasonal Rainfall Time Series in the Mediterranean Area**. International Journal of Climatology, 30, 1538-1546, 2010.
- Mann, H.B.: **Non-parametric tests against trend**, Econometrica 13:163-171, 1945.
- Mehta, A. V., and S. Yang, **Precipitation climatology over Mediterranean Basin from ten years of TRMM measurements**, Advances in Geosciences 17, 87-91, 2008.
- Montaldo N.; Sarigu A.: **Potential links between the North Atlantic Oscillation and decreasing precipitation and runoff on a Mediterranean area**, Journal of Hydrology, 553, 419–437, 2017.

- Piervitali E.; Colacino M.; Conte M.: **Signals of Climatic Change in the Central-Western Mediterranean Basin**, Theoretical and Applied Climatology, 58, 211–219, 1997.
- Schonwiese C.; Rapp J.: **Climate Trend Atlas of Europe Based on Observations 1891–1990**. Kluwer Academic Publishers, Dordrecht, The Netherlands, 1997.
- Xoplaki E.; Luterbacher J.; González-Rouco J.F.: **Mediterranean summer temperature and winter precipitation, large-scale dynamics, trends**, Nuovo Cimento C, 29, 45-54, 2006.

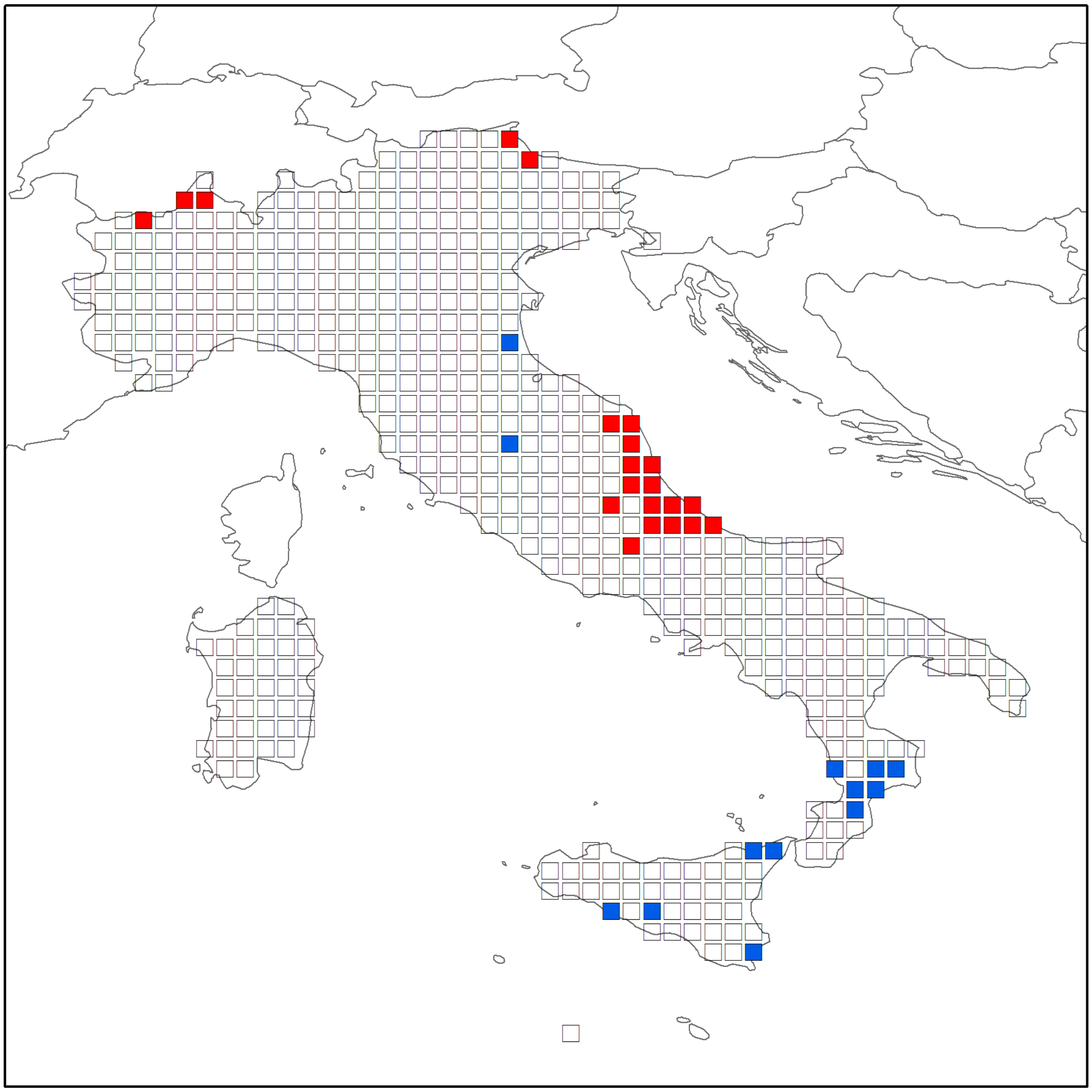

Figure 1 – Results of annual trends.

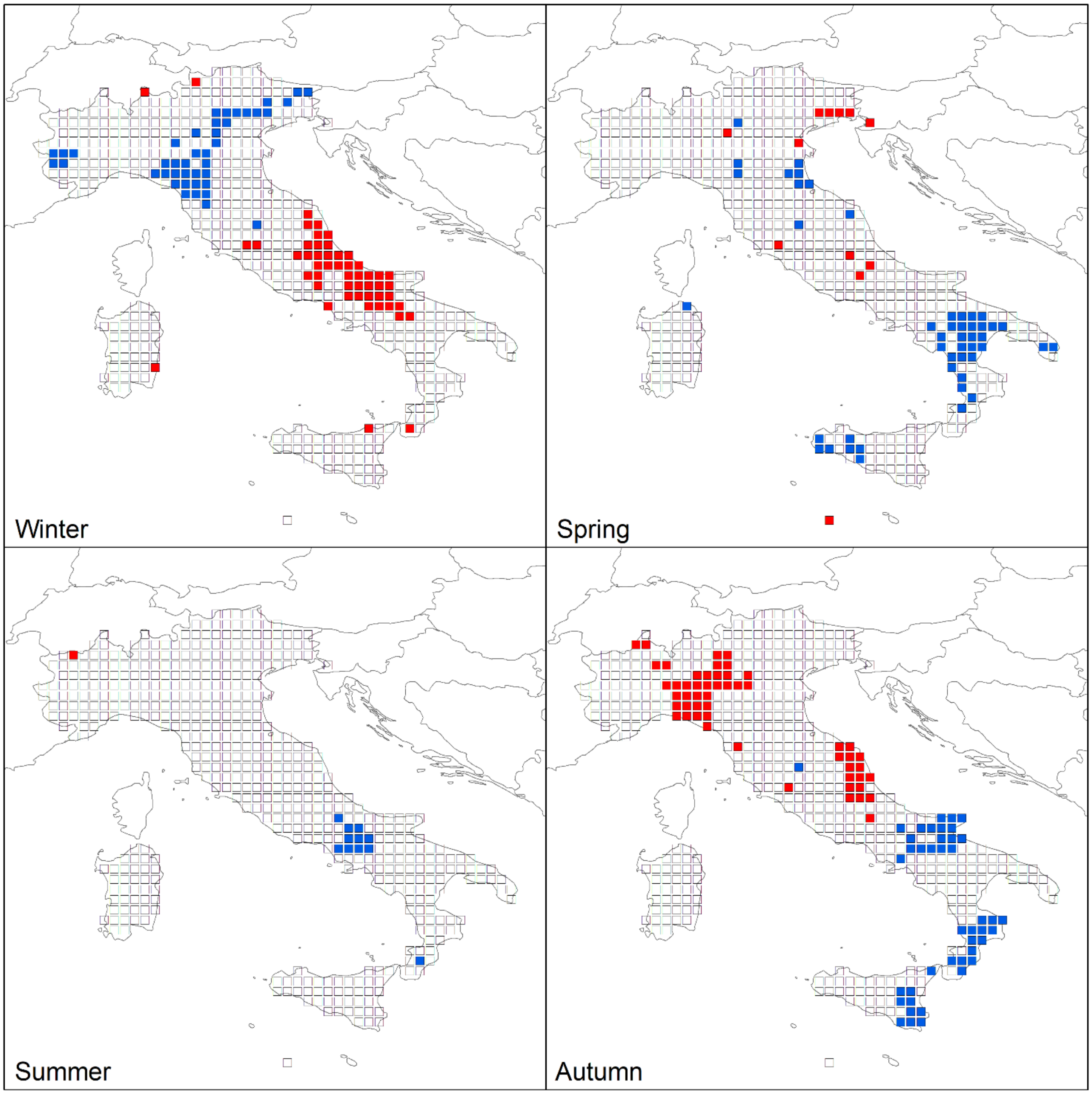

Figure 2 – Results of seasonal trends.

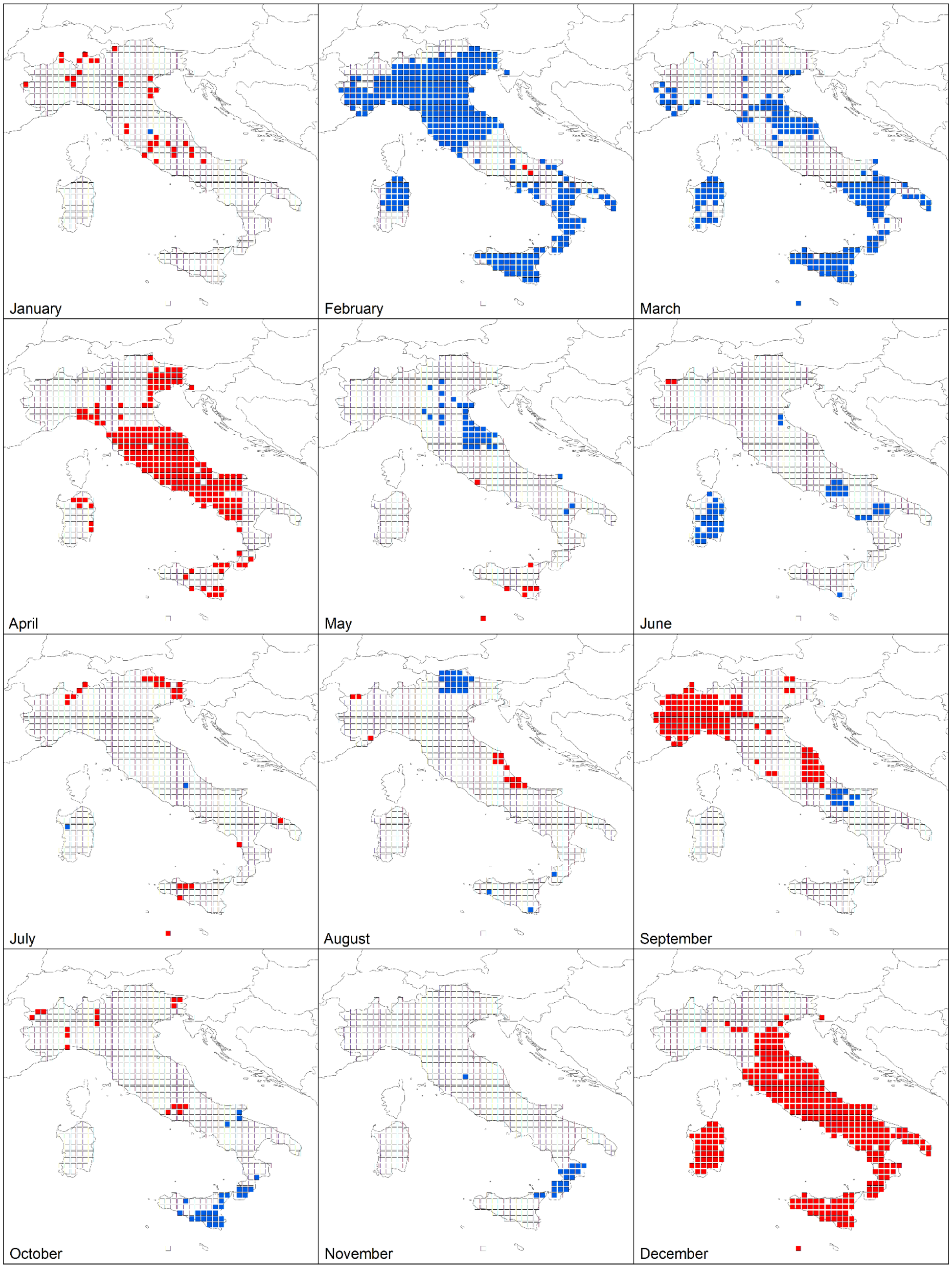

Figure 3 – Results of monthly trends.